Journal of Building Engineering 117 (2026) 114902

Contents lists available at ScienceDirect

Journal of Building Engineering

journal homepage: www.elsevier.com/locate/jobe

Evaluation of aggregate-cement paste Interface: Effects of aggregate characteristics on acid attack and permeability of concrete

Nurdeen M. Altwair [a,*], Ashraf M. Al-Kilani [a], Mustafa M. Al-Tayeb [b], Ramadhansyah Putra Jaya [c]

[a] Civil Engineering Department, Faculty of Engineering, Elmergib University, Khoms, Libya
[b] Department of Civil Engineering, Faculty of Engineering, Hasan Kalyoncu University, Şahinbey, Gaziantep, Türkiye
[c] Faculty of Civil Engineering Technology, Universiti Malaysia Pahang Al-Sultan Abdullah, 26300, Kuantan, Pahang, Malaysia

ARTICLE INFO

Keywords:
Aggregate type and size
Roughness
Interfacial transition zone
Sulfuric acid attack
Water permeability

ABSTRACT

This investigation systematically evaluates the influence of aggregate type (basalt, white limestone, and brown limestone) and nominal size (10, 14, and 20 mm) on the characteristics of the interfacial transition zone (ITZ) and the durability of plain concrete, specifically its acid resistance and water permeability. The experimental program involved a comprehensive characterization approach. Aggregate surface roughness was quantified using a surface profilometer. The ITZ's microstructural and mechanical properties were analyzed via SEM, XRD, and direct tensile testing. Durability was assessed by evaluating acid resistance—determined by mass and compressive strength loss after 30-day immersion in 5 % H_2SO_4—and water permeability, measured in accordance with BS EN 12390–8:2019. The findings revealed that fractured aggregate surfaces significantly enhanced bond strength over sawn counterparts. A key mechanistic insight is that the *nature* of roughness, not just its magnitude, governs performance: naturally fractured aggregates are significantly rougher, with basalt's texture defined by high peaks (promoting mechanical interlocking) and limestone's by deep valleys. Basalt's chemical reactivity further improved the ITZ by consuming portlandite to create a denser, stronger interface, whereas limestone produced a more porous ITZ with unhydrated phases. Consequently, concrete incorporating basalt demonstrated superior acid resistance, with the least strength degradation and lowest permeability. White limestone performed moderately, while brown limestone showed the poorest resistance. Water penetration results aligned with these observations, confirming basalt concrete as the least permeable. For all aggregate types, using smaller sizes effectively mitigated acid damage and reduced permeability. The study underscores basalt's suitability for acidic environments due to its reactivity and ITZ refinement, stressing that aggregate selection and size are critical for designing durable concrete in corrosive conditions.

1. Introduction

The primary component of concrete, coarse aggregate, has a significant effect on the final product due to its inherent properties.

* Corresponding author.
E-mail address: nurdeenaltwair@gmail.com (N.M. Altwair).

https://doi.org/10.1016/j.jobe.2025.114902
Received 2 September 2025; Received in revised form 30 November 2025; Accepted 6 December 2025
Available online 7 December 2025

The specific properties of the coarse aggregate—its origin, size, shape, density, and texture—have a significant impact on the finished concrete's character. The source rock dramatically impacts the physical, mechanical, geological, and mineralogical properties of coarse aggregate [1]. This principle of material selection is foundational and extends to modern concrete technologies, where the strategic use of constituent materials, such as recycling industrial by-products like coal gasification slag, is crucial for developing eco-friendly, high-performance composites with tailored microstructures and mechanical properties [2]. Different aggregates have different effects on concrete's workability, strength, and durability [3]. Their causes could lie in the physical or mechanical realms. The overall strength of concrete may be improved by using diverse aggregates since various types of aggregate significantly affect compressive strength and long-term performance. The aggregate's overall characteristics, including its shape, surface texture, and grading, directly impact the workability, pumpability, granular separation, strength, durability, hardness, creep, shrinkage, density, and permeability of both fresh and hardened concrete [1]. In both the fresh and hardened forms of concrete, the intrinsic features of the parent rock material play a significant role. These attributes include specific gravity, hardness, chemical and mineral composition, resistance, physical rock classification, chemical stability, and porous structure [1,4,5].

Buildings constructed of concrete in extreme environments are affected by its water permeability, which is an important quality of concrete. Because water is both an active ingredient and a solvent, it may dissolve concrete and release toxic substances like chloride and sulfate ions into the mix [6]. Several important factors affect concrete's durability and permeability. Several factors influence concrete, including its compressive strength, water-to-cement ratio, curing methods, age, and aggregate quality [7]. When the water-to-cement ratio is between 0.3 and 0.7, the permeability of the cured cement paste typically ranges from 0.1×10^{-12} to 120×10^{-12} cm/s [8]. The permeability range for common aggregate is between 1.7×10^{-9} and 3.5×10^{-13} cm/s, according to Ref. [8]. Aggregate is generally less permeable than hardened cement paste, depending on their mineral composition. However, aggregate still plays a significant role in the overall permeability of concrete. It is widely believed that increasing the aggregate size increases the permeability for a given water-to-cement ratio, and that well-graded aggregate is required to obtain low-permeability concrete [9]. When the aggregate size is large, there are larger gaps between the particles, creating larger void spaces. This allows water and other materials to penetrate more easily through the cement paste. In contrast, when smaller-sized aggregate is used, the spaces between the particles become smaller, reducing the volume of void spaces, which leads to a decrease in the permeability of water and other material solutions [10]. On the other hand, using a larger aggregate size results in fewer pores in concrete, thereby reducing the available surface area for water permeation. This leads to an increase in the concrete's resistance to water permeability. Conversely, smaller aggregate sizes can result in an increased number of pores and available surface area, leading to higher water permeability [8]. However, this relationship is dependent on various factors, such as cement properties, water-to-cement ratio, aggregate properties, aggregate-to-cement ratio, and the use of admixtures [10]. The pore volume in aggregate typically accounts for around 10 % of the cement paste volume. However, this pore volume can be significantly larger. Therefore, the volume and grading of aggregate in concrete can significantly impact the overall permeability [11]. Additionally, the interfacial transition zone (ITZ) between the aggregate and the cement paste is a weak point in concrete, which can lead to the formation of micro-cracks and increased permeability. The cracks around the aggregate caused by volumetric changes in cement paste can also contribute to increased water permeability [12,13]. Consequently, the permeability of concrete is usually significantly higher than the permeability of cement paste.

Concrete structures are frequently exposed to acidic solutions, including accidental spills or leaks from industrial facilities, biogenic acid attacks in concrete sewage pipes, agricultural and food liquid wastes, and wastewater treatment and biogas plants [14,15]. The concrete is impacted by numerous factors when exposed to acidic solutions, including the aggregate, whether fine or coarse. Therefore, further research into the mechanisms of aggregate deterioration in sulfuric acid-attacked concrete is required. Aggregate is primarily classified as either calcareous or siliceous based on its mineral composition. Because of their high calcium carbonate composition, calcareous aggregates like limestone are particularly susceptible to acid attacks. Because of their high silicon dioxide content, siliceous aggregates like basalt and granite are better able to withstand acid attack [16]. The selection of aggregate type to use in an environment dominated by an acidic medium remains a topic of debate. Some researchers assert the aggregate is the primary concrete component, and the process of concrete deterioration accelerates if the acid first damages the aggregate [17]. The aggregate used to make concrete determines how resistant it is to acidity. Limestone aggregate, for instance, could have a higher acidity level than siliceous aggregate [18]. Siliceous and calcareous (limestone) aggregates are common in concrete, and their general behavior changes when exposed to acidity. The cement compounds are shielded from acid attack and degradation by calcareous aggregates like limestone, which safeguards the concrete structure overall. When an acid attack occurs on concrete, the cement hydration compounds are exposed to corrosion. However, when using calcareous aggregate containing calcium, they react with the acid instead of the cement compounds. This reaction leads to the formation of stable and less corrosive compounds [19]. In addition, siliceous aggregate is considered inert when exposed to an acidic environment, primarily due to the extremely low calcium content in the siliceous aggregate. During an acid attack, the cement paste will detach, leaving the siliceous aggregate exposed on the concrete surface. Studies have shown that when concrete congaing limestone aggregate is exposed to a sulfuric acid solution, the paste around the limestone aggregate exhibits less depth of deterioration compared to the paste surrounding the siliceous rock aggregate [20]. In addition, unlike pastes containing siliceous aggregate, those containing limestone aggregate lose a greater mass when exposed to acetic vinegar. In the aftermath of an attack by acetic acid, limestone aggregate serves as a buffer, slowing the acid's degradation in the cement paste [20]. Soluble salts are produced by acids in concrete; thus, it is ideal to use aggregates with a lower proportion of soluble salts rather than limestone [21–23]. On the other hand, other studies have indicated that siliceous aggregate, such as sandstone, granite, and basalt, are more resistant to the effects of acidic solutions, and only the cement paste phase is damaged because siliceous aggregate is mostly immune to the acid attack [24]. The siliceous aggregate demonstrates a heightened susceptibility to becoming dislodged from the cement paste matrix, owing to the dissolution of the cement paste surrounding them [24]. Visual examination by Miyamoto et al. [25] revealed that exposure to H_2SO_4 solution did not cause aggregate to separate from finished cement paste. Many assumed that this was

due to the presence of insoluble gypsum on the concrete's surface. When a solution of hydrochloric acid was poured into the concrete, the opposite occurred. In this case, surface calcium salts developed on the concrete, which caused the aggregate to come free. Pather et al. [26] investigated three different types of aggregates; the ones that showed the highest acid resistance and the least amount of mass loss were the siliceous-calcareous aggregate (dolerite, amphibolite), the siliceous-aggregate (granite, reef-quartzite, meta-quartzite), and the calcareous aggregate (dolomite). Metaquartzite and granite, high in quartz, demonstrated the greatest acid resistance. Reef-quartzite, dolerite, and amphibolite had moderate resistance, while dolomite was highly susceptible, forming gypsum when exposed to sulfuric acid.

This study addresses a significant gap in current research, which has largely concentrated on the isolated effects of either aggregate type or size on concrete durability, often failing to consider their synergistic interactions and cumulative impact. To fill this void, this research pioneers a systematic investigation into the combined effects of aggregate type (basalt, white limestone, and brown limestone) and nominal size (10, 14, and 20 mm) on the acid resistance and water permeability of plain concrete. The core novelty lies in establishing a mechanistic link between these macro-level performance outcomes and the micro-level characteristics of the aggregate-cement interface. To achieve this, the study begins with a detailed characterization of the interfacial transition zone (ITZ) and aggregate surface topography. This preliminary phase employs profilometry to quantify distinct roughness profiles (e.g., peak-versus valley-dominated textures), alongside a combination of direct tensile testing, SEM, and XRD to analyze the ITZ's mechanical and microstructural properties. The findings are anticipated to provide a more holistic understanding of how aggregate selection and sizing govern concrete durability, offering crucial insights for advancing the development of robust formulations for corrosive and challenging service environments.

2. Experimental investigation

2.1. Raw materials

The cement used in the experiments was obtained from El-Mergib Cement Plant, Al-Kums, Libya. Chemical analysis of OPC is shown in Table 1. For the preparation of concrete mixtures, potable water was utilized, exhibiting a total dissolved solids content of less than 2000 ppm. The sand employed in the formulation of the concrete mixtures was sourced from the city of Misurata and constituted natural sand free of impurities. The physical properties of this sand were in conformance with the British Standard BS812-2000, with a specific gravity of 2.61 and a water absorption rate of 2.8 %. The present investigation employed three distinct types of coarse aggregate: basalt, pure white limestone, and brown limestone (Fig. 1). The brown hue exhibited by the brown limestone aggregate is attributable to the presence of impurities, such as clay or mineral contaminants, including iron oxides. For the purposes of this study, the coarse aggregate types were designated as follows: basalt, white limestone, and brown limestone. Table 1 presents the chemical composition of the aggregates as determined by X-ray fluorescence (XRF). The physical characteristics of these three coarse aggregate varieties are detailed in Table 2. The nominal size range of the coarse aggregate utilized in this research was specified between 20 mm and 5 mm. Aligned with the requirements of the current investigation, the nominal size of the coarse aggregate was further subdivided into three distinct gradations: 10 mm (5-10), 14 mm (10–14), and 20 mm (14–20) (Fig. 2).

2.2. Mixtures design and specimen preparation

The ITZ characteristics between various aggregate and cement paste were initially evaluated using cement paste with a 0.47 water-to-cement ratio. To assess the interfacial bond integrity between aggregates and cement paste, a series of tensile bond strength experiments were conducted. The methodology, including specimen dimensions and testing protocol, adhered to the framework established by Jebli et al. [27]. Aggregate prisms, measuring 10 x 10 × 20 mm, were prepared (Fig. 3a). These samples were categorized according to their surface texture into two distinct groups: those with naturally fractured surfaces, which exhibit the aggregate's typical roughness, and those with saw-cut surfaces, prepared by cutting the material with a rock saw (Fig. 3b and c). The primary purpose of the saw-cut specimens is to serve as a controlled reference against which the performance of the naturally fractured surfaces

Table 1
Chemical composition of the OPC and aggregates.

Composition	Percentage composition by mass			
	OPC	Basalt	White limestone	Brown limestone
SiO_2	20.01	50.23	1.60	2.17
Al_2O_3	2.67	10.41	0.32	0.12
Fe_2O_3	4.4	13.96	0.07	2.56
CaO	63.4	9.13	54.13	50.11
MgO	1.56	6.56	0.82	0.72
Na_2O	1.86	2.26	0.26	0.27
K_2O	0.23	0.75	0.08	0.10
SO_3	1.03	0.10	0.11	0.32
P_2O_5	0.13	2.66	0.05	0.06
LOI	1.83	0.15	38.16	41.63
Total	97.12	96.21	95.60	97.79

Fig. 1. Coarse aggregate types: (a) basalt, (b) white limestone, and (c) brown limestone.

Table 2
Physical characteristics of the coarse aggregates.

Property	Type of aggregate			Specification limit in ASTM
	Basalt	White limestone	Brown limestone	
Specific gravity	2.79	2.72	2.69	Min. 2.5
Absorption (%)	0.58	1.12	1.28	Max. 3 %
Unit weight (kg/m3)	1631	1534	1422	1200–1750
Crushing value (%)	14.28	19.33	20.95	Max. 30 %
Los Angeles abrasion (%)	17.48	20.36	21.48	Max. 40 %

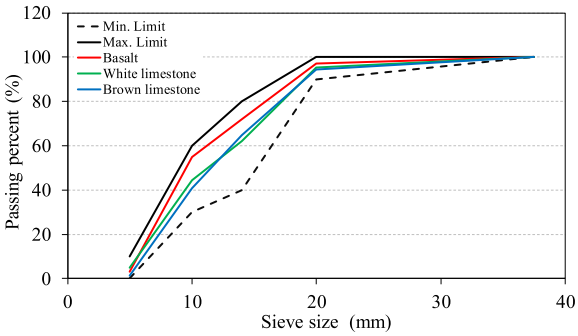

Fig. 2. Particle size distributions of three different types of coarse aggregate.

can be evaluated. By providing a standardized and minimally textured surface, the saw-cut samples make it possible to isolate and quantify the specific contribution of the aggregate's natural surface roughness to the overall tensile bond strength. This comparison allows for a clearer distinction between the chemical adhesion and the mechanical interlocking components of the bond.

For each surface type, a cement paste layer, approximately 2 mm in thickness, was applied between aggregate prism pairs using a Perspex mold. The assembled specimens underwent compaction on a jolting table to ensure uniform contact. To maintain moisture and prevent early-age shrinkage and cracking at the ITZ, specimens were covered with a wet cloth and a polythene sheet for 24 h. Following demolding, the samples were wrapped in a wet cotton cloth, sealed in polythene bags, and cured in a mist room at a controlled temperature of 23 ± 3 °C until testing (Fig. 3d). At 28 days, the tensile bond strength was evaluated under direct tension on saturated surface-dry specimens to avoid leaching and minimize shrinkage-induced stresses at the ITZ. In addition, for the characterization of the aggregate surface roughness, random samples were procured from the same batch of samples utilized in the assessment of the ITZ characteristics between the aggregate and cement paste. The quantification of surface roughness was subsequently performed using a surface profilometer. From the resultant surface profiles, key amplitude parameters were extracted, including: the maximum roughness depth (R_{max}), roughness average (R_a), maximum profile valley depth (R_v), average maximum height of the profile (R_z), and maximum profile peak height (R_p).

To evaluate the impacts of aggregate type and size on concrete's acid resistance and water permeability, a specific mixture was utilized. This comprised 396 kg/m^3 cement, 185 kg/m^3 water, 448 kg/m^3 fine aggregate, and 1344 kg/m^3 coarse aggregate, and the mix targeted a 30 MPa compressive strength. The coarse aggregate component of this reference mixture was substituted by volume with three distinct aggregate types: basalt (B), white limestone (WLS), and brown limestone (BLS). Furthermore, three different

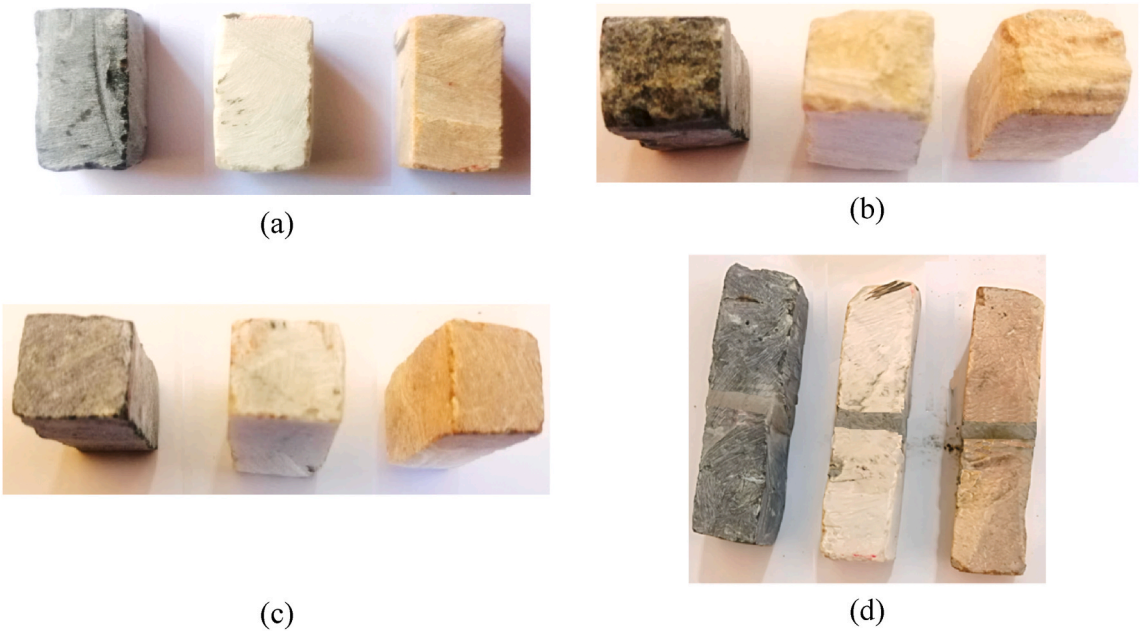

Fig. 3. Preparation of direct tensile test samples: (a) aggregate specimen geometry, (b) fractured surfaces, (c) saw-cut surfaces, and (d) standard test specimen.

aggregate sizes, namely 10 mm, 14 mm, and 20 mm, were incorporated, resulting in a total of 9 unique concrete mixture compositions. For each concrete mixture, 8 cube specimens measuring 150 mm in size were cast, yielding an overall target specimen of 72 cubes. The concrete specimens were mixed in three equal parts and then crushed on a vibrating table to get a consistent density. Shortly after casting, the specimens were wrapped with burlap and put in the controlled casting environment. Specimens were taken out of their molds and cured for the usual 28 days following casting in a water bath maintained at a temperature of 23 ± 3 °C. Next, a 5 % sulfuric acid solution was used to evaluate the acid resistance of 36 cubes, while the other 36 specimens were subjected to standardized permeability tests.

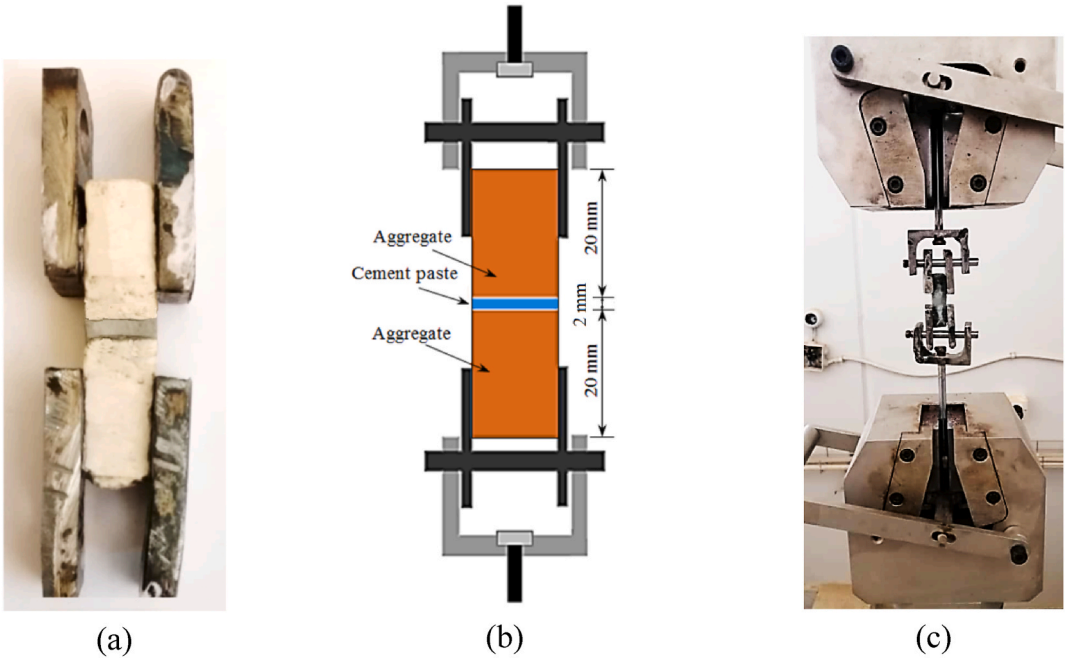

Fig. 4. Direct tensile test: (a) attaching metal shims to the specimen, (b) test schematic, and (c) experimental setup.

2.3. Test methods

2.3.1. ITZ characteristics assessment tests

The tensile bond strength between cement paste and aggregate particles was measured though direct tensile test using a Universal Testing Machine (UTM) at a displacement rate of 0.6 mm/min. The experimental setup was designed to accommodate the size and geometry of the specimen depicted in Fig. 3d. Initially, four metal shims with pre-drilled holes were affixed onto the specimen, as illustrated in Fig. 4a. In order to conduct the test, the specimen was secured by inserting metal rods through the shim holes and into the U-shaped support mounted on the testing machine (Fig. 4b and c). Fractured surfaces post-direct tensile testing were utilized to analyze ITZ mineral phases. ITZ material, comprising cement-paste aggregate combinations, was carefully scraped, and the resulting powder subjected to XRD analysis. Scraping was performed within 2 mm of the aggregate surface to isolate the cement paste. Additionally, SEM was performed on these same fracture surfaces to qualitatively examine the ITZ's microstructure. Since the direct tensile test induces failure along the ITZ, these surfaces represent the actual failure plane, revealing its topography rather than a polished cross-section. This method provides a direct view of the features contributing to bond failure. The identification of specific hydration products, such as ettringite, was based on their distinct and well-documented crystal morphologies (e.g., acicular shapes), as well as the plate-like appearance of Calcium hydroxide.

2.3.2. Testing for resistance against sulfuric acid

A 5 % sulfuric acid solution was prepared in an acid-resistant tank and maintained at an ambient temperature of 23 ± 3 °C. After 28 days of curing, specimens were dried for 30 min to remove surface moisture, and their initial saturated surface-dry masses were precisely recorded. Specimens were then continuously immersed in the 5 % sulfuric acid solution for a duration of 30 days [28].

The selection of a 30-day immersion period in a 5 % sulfuric acid solution represents a highly accelerated testing protocol. This approach was intentionally chosen to induce significant and measurable degradation, enabling a clear comparison of the performance of concretes made with basalt, white limestone, and brown limestone within a practical timeframe. While standards like ASTM C1898/C1898M − 22 provide for longer exposure durations (e.g., 56 and 84 days), the high acid concentration used in this study makes such extended periods problematic. Prolonged exposure would likely cause excessive material loss, potentially compromising the reliability of post-exposure mechanical tests, such as compressive strength and mass losses evaluation. Thus, the 30-day duration was considered an optimal balance to evaluate the relative acid resistance linked to aggregate type and size, which is the primary focus of this investigation.

To ensure uniform exposure, specimens were carefully distributed within the solution, and containers were sealed with a plastic film to prevent evaporation. The solution was replenished every 5 days to maintain its concentration. Following the 30-day immersion, specimens were rinsed with tap water without brushing, visually examined, and weighed [29]. They were then dried at room temperature for 30 min. Finally, the cumulative mass change (W_C) was calculated for each specimen relative to its initial mass:

$$W_C = \frac{W_{30} - W_0}{W_0} \times 100 \quad (1)$$

where, W_{30} is the mass of the specimen 30 days of immersing (kg), and W_0 is the initial mass of the specimen before exposure to sulfuric acid (kg).

An essential part of the experimental investigation was determining how the acid solution affected the decrease in compressive strength. As a part of this investigation, all specimens were subjected to residual compressive strength testing, which considered the original cross-sectional area. Following this, the percentage change in strength was calculated using an approach similar to the mass alteration equation given before.

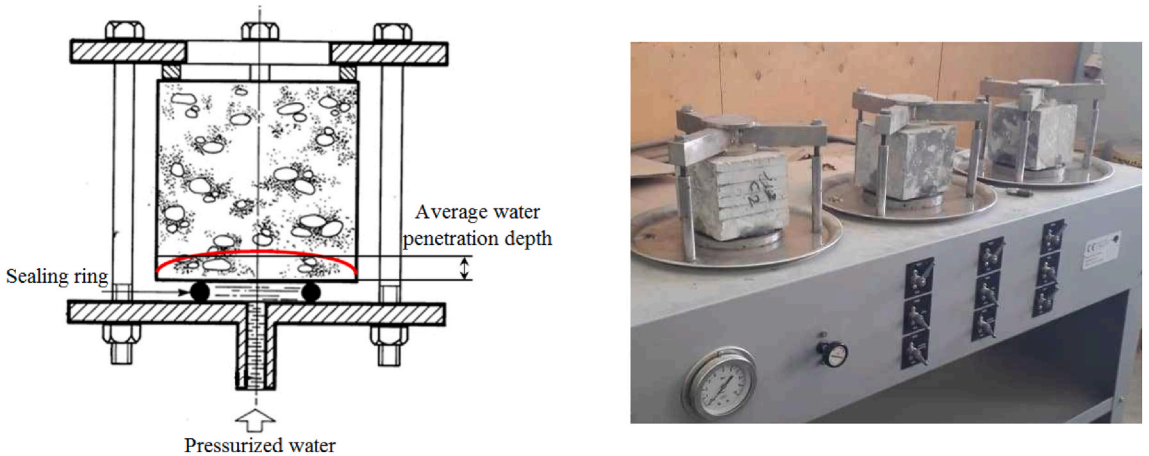

Fig. 5. Graphical representation and experimental set-up for permeability testing.

To evaluate the progression of sulfate attack, a phenolphthalein colorimetric test was employed. This analytical technique was used to assess the depth of sulfuric acid penetration into the test specimens. When the pre-prepared phenolphthalein solution was applied, a distinct pink color indicated a pH greater than 8.5, signifying substantial alkalinity and a negligible impact from the sulfuric acid exposure. Conversely, colorless regions denoted a pH below 8 and the presence of reaction products from the chemical interactions [30]. The phenolphthalein solution was uniformly applied to the split surfaces of the specimens to measure the depth of sulfuric acid infiltration within the specimen interfaces.

2.3.3. Water permeability test

In accordance with the British Standard BS EN 12390–8:2019, water permeability testing was performed on the concrete specimens following a 28-day curing period. As illustrated in Fig. 5, the experimental procedure involved positioning the test specimens within the purpose-built permeability cells. Water was then applied to the lower face of each specimen under a constant vertical pressure of 7 bar (700 kPa), which was sustained for a continuous duration of 72 h. Upon completion of the testing period, the specimens were split vertically in a direction perpendicular to the applied water pressure on the lower face. The depth of water penetration was then measured precisely to the nearest millimeter. Based on the results of this assessment, the water permeability coefficient (kw) was calculated using the formula provided in Eq. (2) [31].

$$k_w = \frac{d^2 \nu}{2ht} \tag{2}$$

where:

k_w is the coefficient of water permeability (in m/s)
d is the depth of water penetration into the concrete in meters (m)
h is the hydraulic head in meters (m)
t is the time under pressure in seconds (sec.)
ν is the porosity of the concrete, determined using Eq. (3).

$$\nu = \frac{m}{Ad\rho} \tag{3}$$

where:

m is the gain in mass of the specimen in kilograms (kg)
A is the cross-sectional area of the specimen in square meters (m^2)
ρ is the density of water in kilograms per cubic meter (kg/m^3)

3. Results and discussion

3.1. Aggregate surface roughness assessment

To ensure the representativeness of the results and to mitigate potential measurement bias, a systematic and rigorous measurement protocol was implemented. For each of the three aggregate types (basalt, white limestone, and brown limestone), nine particles were randomly selected from the bulk sample. Measurements were conducted on both saw-cut and naturally fractured surfaces, with distinct protocols tailored to their topographical characteristics. Considering the relatively uniform texture of the saw-cut surfaces, surface roughness was characterized by scanning two orthogonal profile lines on each particle. Consequently, the surface roughness parameters were averaged over these two lines (Table 3).Conversely, for the more heterogeneous fractured surfaces, four distinct measurement zones were identified per particle to ensure comprehensive coverage of surface variability. These zones were strategically distributed to counteract sampling bias: two zones were located on relatively flat faces, while the other two were deliberately positioned on pronounced angular edges and corners. Within each measurement zone, two parallel profile lines, each 5 mm in length, were scanned. The final roughness value for a single particle was determined by averaging all its constituent measurements (e.g., 8 measurements for a fractured surface). Subsequently, the overall surface roughness parameters for each aggregate type (Table 3) were calculated as the arithmetic mean of the corresponding parameters derived from the nine individual particle averages. Fig. 6 illustrates a selection of models representing surface profiles for three distinct aggregates: basalt, white limestone, and brown limestone,

Table 3
Surface roughness parameters of different aggregate types.

Surface parameters (μm)	Basalt aggregate		White limestone aggregate		Brown limestone aggregate	
	Saw-cut surface	Fractured surface	Saw-cut surface	Fractured surface	Saw-cut surface	Fractured surface
R_a	7	84	4	70	5	59
R_v	19	72	13	110	15	126
R_{max}	40	240	20	198	32	230
R_z	38	213	25	176	27	208
R_p	22	168	13	148	17	139
R_{sk}	+0.03	+0.34	+0.01	+0.25	+0.01	+0.11

evaluated under both saw-cut and naturally fractured conditions.

The data presented in Table 3 provides critical insights into how both the aggregate material type and the surface preparation method fundamentally influence surface topography. The most prominent and immediate observation is the stark contrast between the saw-cut and fractured surfaces across all three aggregate types. Without exception, the fractured surfaces exhibit roughness parameters (R_a, R_v, R_{max}, R_z, R_p, and R_{sk}) that are significantly, often an order of magnitude, higher than their saw-cut counterparts. For instance, the arithmetic mean roughness (Ra) for fractured basalt is 84 μm, which is precisely 12 times greater than its saw-cut value of 7 μm. Similarly, white limestone shows an even more dramatic increase, with its fractured R_a value (70 μm) being 17.5 times higher than its saw-cut value (4 μm). This profound disparity underscores the fundamental difference between the two preparation methods: a saw-cut surface is the product of a controlled, mechanical abrasion process that yields a relatively smooth and uniform low-relief profile, whereas a fractured surface is the result of natural fracture mechanics, which creates an irregular, complex, and high-relief topography by propagating cracks along the material's intrinsic planes of weakness. This universal trend confirms that fracturing is a highly effective method for inducing significant surface roughness, a key factor for enhancing mechanical bonding in composite materials like concrete.

When comparing the fractured surfaces, which represent the intrinsic textural properties of the materials themselves, more nuanced and revealing characteristics emerge. While the basalt aggregate displays the highest overall average roughness ($R_a = 84$ μm),

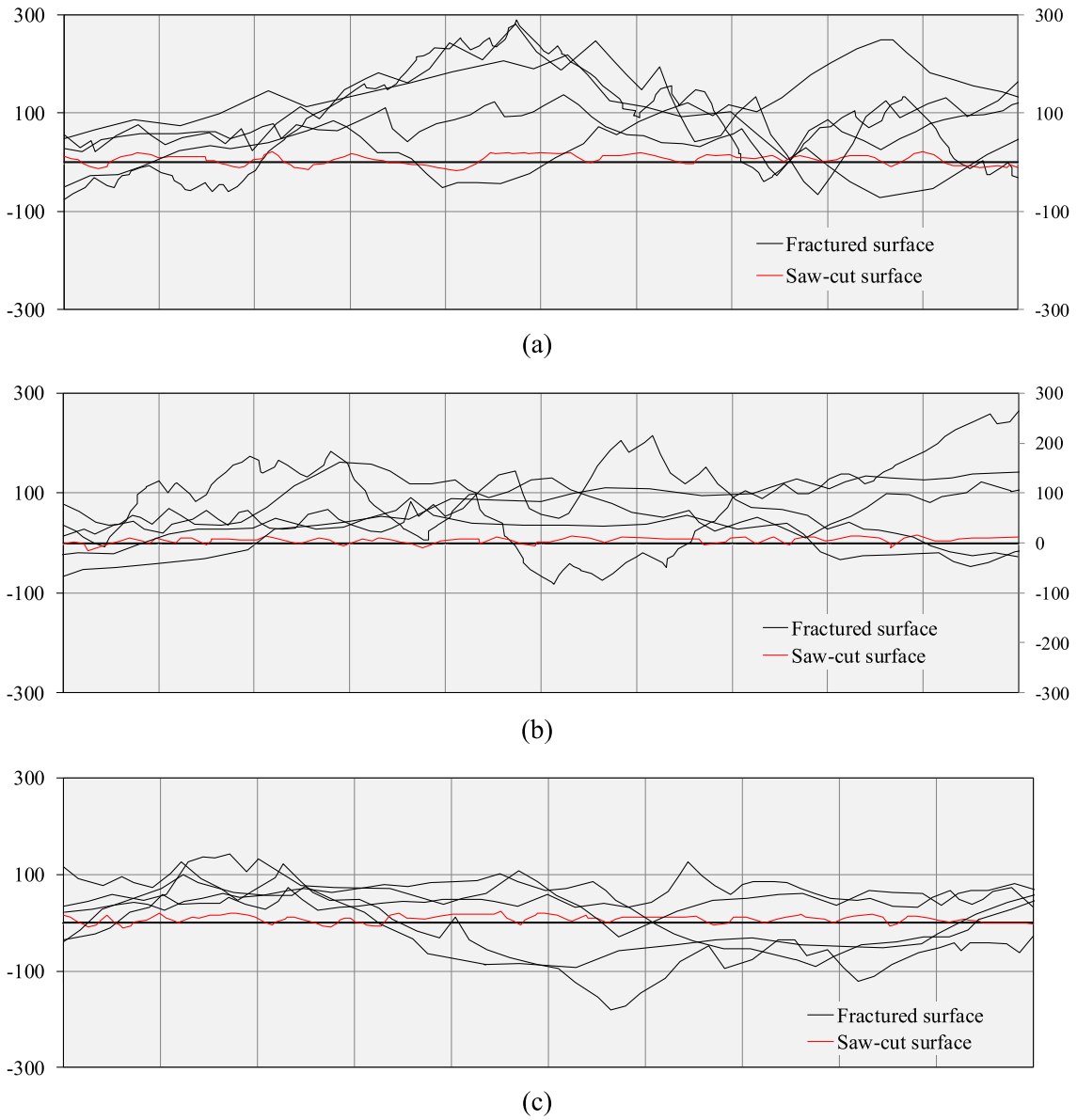

Fig. 6. Selection of models illustrating the surface profiles for (a) basalt, (b) white limestone, and (c) brown limestone.

suggesting a uniformly rugged texture, a deeper analysis of the profile components reveals the true nature of each surface. The most interesting insight is found by deconstructing the roughness values into their constituent peaks (R_p) and valleys (R_v). The basalt's high roughness is predominantly driven by its exceptionally high peaks, registering the maximum peak height ($R_p = 168$ μm) among all fractured samples, while its valley depth ($R_v = 72$ μm) is the shallowest. This is further confirmed by its high skewness value ($R_{sk} = +0.34$), the largest in the dataset, which mathematically indicates a profile dominated by sharp, high asperities rising above a relatively flatter mean line. In stark contrast, the limestone aggregates exhibit a topography defined by their valleys. Brown limestone, in particular, registers the deepest average valleys ($R_v = 126$ μm) and the highest maximum peak-to-valley height ($R_{max} = 230$ μm, second only to basalt), yet its peak heights ($R_p = 139$ μm) and overall average roughness ($R_a = 59$ μm) are the lowest. This indicates a surface morphology characterized by deep gorges and chasms rather than high, sharp peaks. The white limestone presents a similar, albeit less extreme, valley-dominated profile. Therefore, while fracturing invariably enhances surface roughness, the nature of this roughness is highly material-dependent. Basalt's topography is characterized by high-amplitude peaks, whereas limestone's roughness is driven by the presence of deep, significant valleys. These distinct characteristics are critical for understanding the mechanical interlocking potential at the interfacial transition zone (ITZ) with cement paste, as a peak-dominated surface may provide different bonding mechanisms compared to a valley-dominated one.

3.2. Characteristics of the ITZ between aggregate and cement paste

Fig. 7 depicts the tensile bond strength between cement paste and different aggregate types, accounting for both sawn and fractured surface characteristics of the aggregate. The three aggregate types demonstrated significant variations in their influence on the bond strength at the aggregate-cement paste interface. Notably, each result is an average of three specimens, with all coefficients of variation remaining below 9 %. Consistently, fractured surfaces, indicative of greater surface roughness, yielded superior tensile bond strength across all aggregate types when compared to saw-cut surfaces. This suggests that bond strength increases with enhanced surface roughness, irrespective of the aggregate type. Fractured aggregate surfaces achieve higher tensile bond strength than saw-cut surfaces primarily due to two factors. Firstly, their irregular nature provides a greater surface area for adhesion with the cement paste. Secondly, and crucially, their rough topography facilitates superior mechanical interlocking, where the cement paste physically keys into the aggregate's surface texture. This "interlocking by the aggregate surface texture" creates a more robust and stronger bond [32,33]. However, the results indicated that basalt aggregate has a considerably more significant effect on tensile bond strength when contrasted with both white and brown limestone aggregates. Furthermore, the brown aggregate surface was consistently found to yield the minimum bond strength among the tested variants. The basalt-cement paste interfacial tensile bond strength was 3.45 MPa for fractured surfaces and 2.73 MPa for saw-cut surfaces. Comparatively, these respective strengths were 2.95 MPa and 2.48 MPa for white limestone, and 2.48 MPa and 2.26 MPa for brown limestone.

Direct tensile testing revealed four distinct failure modes: Type A involved fracture localized within the ITZ. Type B was characterized by ITZ failure with associated cement paste debonding. Type C exhibited ITZ failure accompanied by aggregate fracture. Finally, Type D demonstrated predominantly cement paste failure with minimal ITZ involvement. Fig. 8a illustrates the distinct failure modes observed in the direct tensile tests after washing and removing loose fragments, which varied according to aggregate type and surface roughness. Basalt aggregate specimens exhibited Type B failure on saw-cut surfaces and Type D failure on fractured surfaces. The Type D mode, in particular on fractured surfaces, correlated with a significant enhancement in direct tensile strength. Conversely, white limestone aggregate specimens consistently presented Type B failure across both saw-cut and fractured surface topographies, as depicted in Fig. 8b. This behavior corresponded to a comparatively lower direct tensile strength than that observed for basalt aggregates. Furthermore, brown limestone specimens displayed Type A failure on saw-cut surfaces and Type C failure on fractured surfaces. These patterns, especially Type A and C for brown limestone, are indicative of a compromised aggregate-cement paste interfacial bond strength (Fig. 8c). The delineated failure modes thus reflect the varying tensile strength characteristics of the aggregate-cement paste interfacial zone. However, the superior tensile strength of basalt specimens is attributed to their firmer and

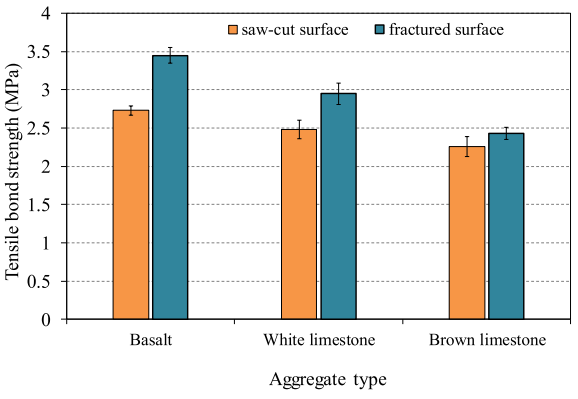

Fig. 7. Tensile bond strength between various aggregate types and cement paste with differing surface roughness.

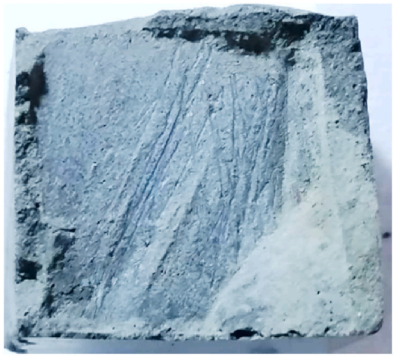

Type B failure mode on saw-cut surface

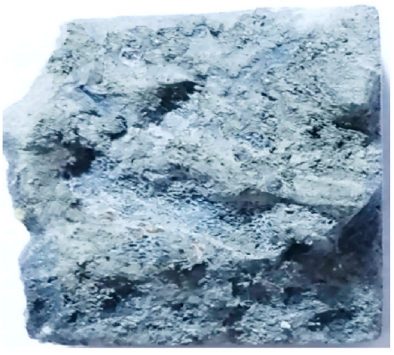

Type D failure mode on fractured surface

(a)

Type B failure mode on saw-cut surface

Type B failure mode on fractured surface

(b)

Type A failure mode on saw-cut surface

Type C failure mode on fractured surface

(c)

(caption on next page)

Fig. 8. Modes of bond failure in direct tensile test: (a) basalt, (b) white limestone, and (c) brown limestone.

more robust crystalline structure compared to limestone, which lacks significant zones of weakness. This property enables the fractured basalt surface to attain enhanced interfacial bond strength with the cement paste [34]. The inherent mineralogical, structural, and textural properties of the basalt aggregate made it better able to develop and maintain a strong interfacial bond with the cement paste compared to the limestone aggregate.

Post-tensile split surfaces in the ITZ were assessed using SEM imaging at 28 days. An investigation detailed in Fig. 9 reveals that white limestone and brown limestone aggregates exert a considerable impact on the attributes and characteristics of the microstructural development within the ITZ, particularly when contrasted with basalt aggregate. The analysis indicates that the ITZ at the cement paste interface adjacent to the limestone aggregate surface is notably defined by a significantly elevated level of porosity, which can be visually observed as dark spots ranging from 25 to 100 μm in size (Fig. 9a). This pronounced porosity suggests a potentially weaker bond and altered transport properties in this critical region. According to Tasong et al. [35], the formation of pores in the ITZ between limestone and cement paste primarily results from carbon dioxide emitted during their chemical reaction. This release, which was verified through its effect on limewater, suggests the creation of weak acidic pockets from poorly crystalline silica interacting with calcite, ultimately leading to increased porosity in the ITZ. Reduced hydration product formation was evident at the limestone/cement matrix ITZ. This was accompanied by needle-like radiating crystals and a limited quantity of calcium hydroxide (CH) within the pores (Fig. 9b). Furthermore, a distinct concentration of CH was observed in the non-porous regions of the ITZ (Fig. 10). In stark contrast, the ITZ of the basalt/cement matrix was dense and well-compacted. This superior microstructure is attributed to a dual mechanism. First, the high-peak roughness of basalt provides excellent mechanical interlocking. Second, a pozzolanic reaction occurs between the reactive silica and alumina in the silicon-rich basalt and the portlandite (CH) from cement hydration [35]. This secondary reaction consumes the weak, plate-like CH crystals and produces additional, dense calcium silicate hydrate (C-S-H), effectively filling pores and densifying the ITZ. Additionally, fracture surfaces within the basalt ITZ exhibited a network of fine ettringite crystals on the aggregate side (Fig. 11), indicating enhanced microstructural densification through supplementary reaction mechanisms. The SEM analysis in this study aligns with Kong and Du [36], who demonstrated that cement paste surrounding limestone exhibits a weak microstructure characterized by abundant porosity. They identified reaction traces between basalt aggregate and cement paste, indicating a chemical interaction that generates a denser interfacial microstructure compared to

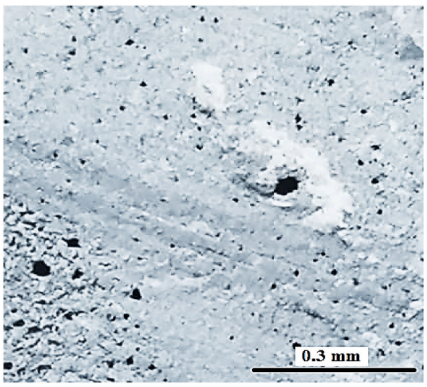

(a)

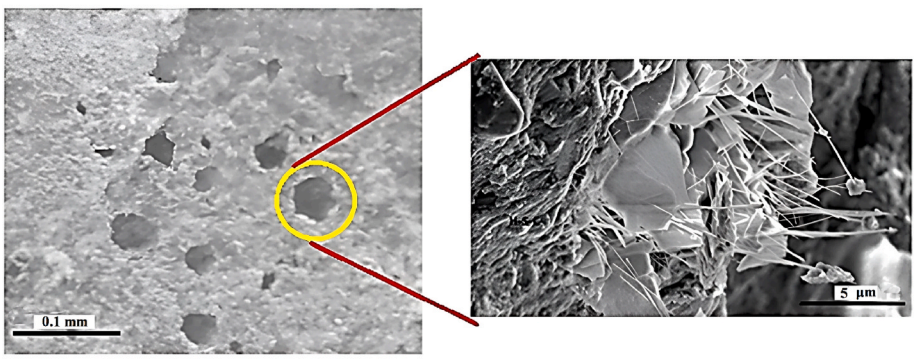

(b)

Fig. 9. ITZ between limestone aggregate and cement paste: (a) pore distribution at the ITZ around the limestone aggregate surface, (b) high-magnification SEM image of interfacial porosity.

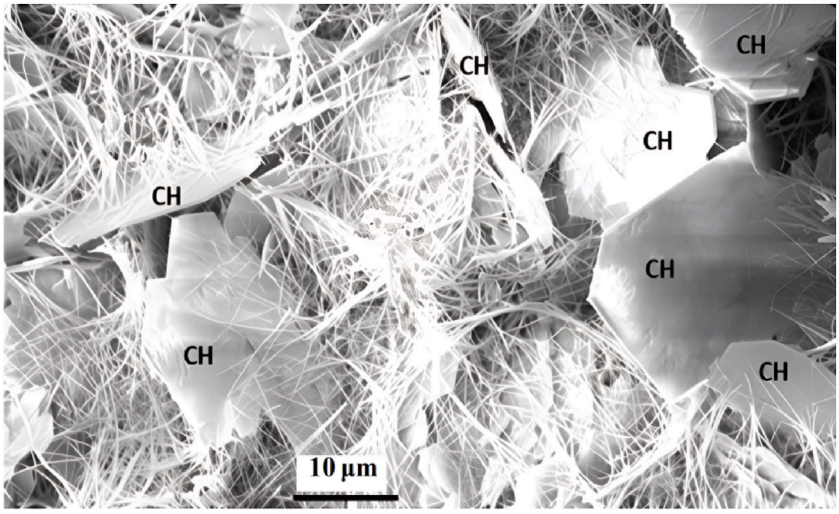

Fig. 10. Calcium hydroxide in the cement paste-limestone ITZ.

limestone. This densification manifests as minor pores, localized defects, and tightly aggregated hydrate clusters within the basalt-cement matrix.

A comparison of the XRD patterns (Fig. 12) demonstrates that hydration products at the cement paste-aggregate ITZ vary across aggregate types after 28 days of curing. It is evident that the primary compounds present are portlandite (CH), alite (C_3S), and belite (C_2S), along with other hydration products such as calcium aluminate hydrate compounds. In cement paste powder around limestone, C_3S and C_2S are abundant, unlike basalt-adjacent paste, which shows minimal unhydrated clinkers. Furthermore, XRD analysis reveals a noticeable presence of CH with distinct peaks in the limestone ITZ, contrasting with the less pronounced peaks in the basalt ITZ, indicating a lower CH content. This finding provides strong evidence for the proposed mechanistic difference: the lower CH content in the basalt ITZ confirms its consumption through the pozzolanic reaction, leading to the formation of more stable C-S-H and a refined, stronger interface. Conversely, the high CH concentration in the limestone ITZ signifies a more traditional, weaker interface dominated by large, oriented CH crystals. This heightened chemical activity of basalt relative to limestone, as established by the reduced CH and increased clinker hydration, is a critical factor in its superior performance. Critically, XRD test results confirm the findings obtained from the SEM analysis.

3.3. Assessment of acidic effects

Concrete is particularly vulnerable to sulfuric acid's acid and sulfate attacks. All of the concrete specimens are affected by the acid assault that starts when the specimens are submerged in the sulfuric acid solution. This effect is evidenced by the clear emergence of air bubbles rising to the surface of the solution. The direct appearance of these bubbles serves as a strong indicator of the initiation of the chemical reaction between the acid and the concrete specimens. In fact, sulfuric acid will chemically react with the compounds formed during the cement hydration process, leading to the formation of soluble reaction products [37]. It was observed that after the first week of exposure, a dense white precipitate, specifically identified as gypsum, was deposited on the surface of the concrete specimens.

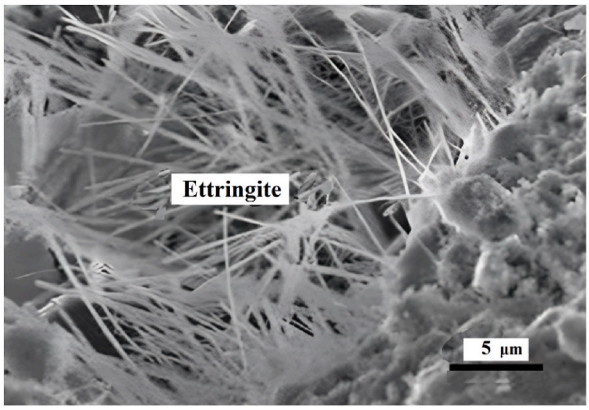

Fig. 11. Ettringite crystal network in the basalt aggregate-cement paste ITZ.

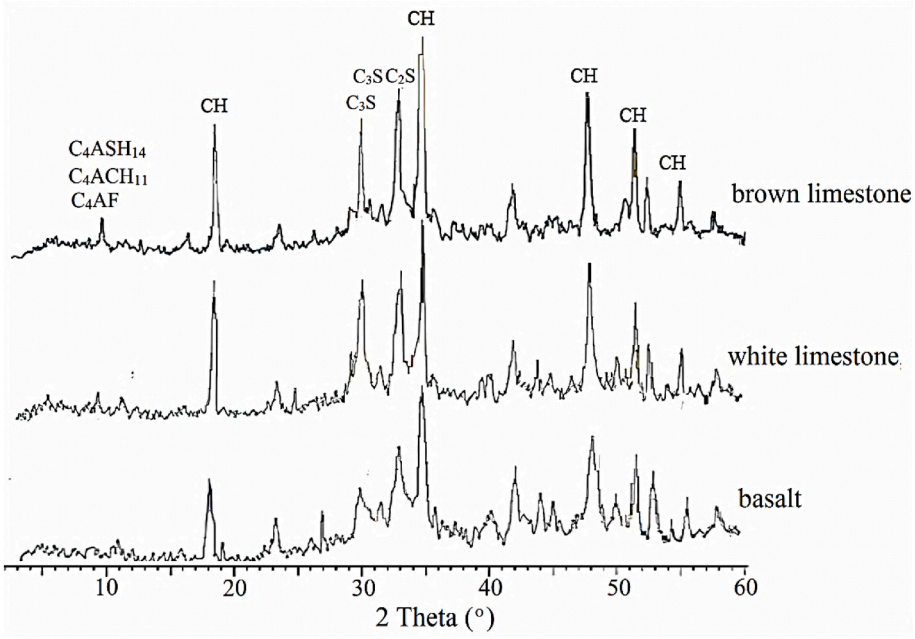

Fig. 12. X-ray powder diffraction patterns of the products formed at the ITZ between the cement paste and various types of coarse aggregates after 28 days of curing. CH = calcium hydroxide (portlandite); C_4ASH_{14} = tetracalcium aluminate monosulfate- 14-hydrate; C_4ACH_{11} = tetracalcium aluminate carbonate- 11-hydrate; C_4AF = tetracalcium aluminoferrite; C_3S = Alite; C_2S = belite.

This gypsum layer gradually increased in thickness over time. As the gypsum was continuously added to the container, the silt at the base became white, like freshly mixed cement paste. The first stage involves the production of gypsum byproduct of the hydration of cement and the breakdown of calcium hydroxide. The more expansive consequence of the gypsum's chemical interaction with the calcium sulfoaluminate in the water is ettringite. The formation of this ettringite combination applies internal pressure to the concrete matrix, causing cracks and the material to transform into a mushy, incoherent mass. Additionally, sulfuric acid may also remove lime from the calcium silicate hydrates, eventually converting them into amorphous hydrous silica. The following chemical equations represent these reactions [38]:

$$Ca(OH)_2 + H_2SO_4 \rightarrow CaSO_4 \cdot 2H_2O \text{ (Gypsum formation)}$$

$$CaSO_4 \cdot 2H_2O + 3CaO \cdot Al_2O_3 \cdot 6H2O \rightarrow 3CaO \cdot Al_2O_3 \cdot 3CaSO_4 \cdot 32H_2O \text{ (Ettringite formation)}$$

$$xCaO \cdot SiO_2 \cdot yH_2O + H_2SO_4 \rightarrow SiO_2 \cdot nH_2O + CaSO_4 \text{ (Silicate hydrate decomposition)}$$

The formation of gypsum on the concrete surface and its subsequent deposition can lead to the clogging of the pores present on the specimen's surface. This pore-blocking mechanism results in an initial slowing of the acid attack rate. However, this mitigating effect is only temporary in nature [39].

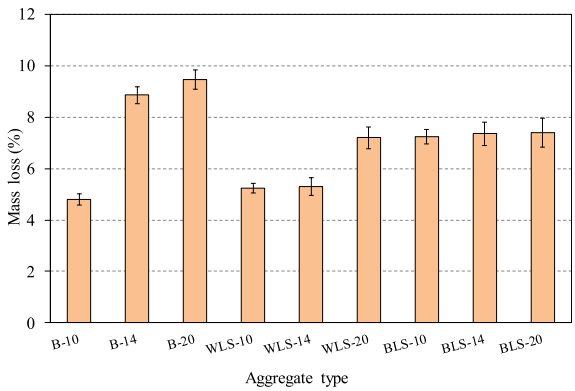

Fig. 13. Effect of aggregate type and size variations on mass loss.

3.3.1. Mass loss

The majority of established studies regard mass loss as an accepted indicator for evaluating the resistance of concrete to sulfuric acid attack [40]. The data presented in Fig. 13 reveals that significant effect of aggregate size on mass loss upon exposure to a 5 % sulfuric acid solution over a 30-day period. Across the various aggregate types examined, an increase in particle size consistently corresponded with a higher degree of mass reduction. For basalt aggregate, the mass loss percentages were approximately 4.8 %, 8.85 %, and 9.45 % for sizes of 10, 14, and 20, respectively. Similarly, white limestone (WLS) aggregate exhibited mass loss around 5.25 %, 5.3 %, and 7.2 % for the corresponding size ranges, while brown limestone (BLS) showed mass loss of roughly 7.25 %, 7.35 %, and 7.4 %. This trend of increasing mass loss with greater aggregate size was most pronounced for the basalt specimens, followed by the WLS and BLS aggregate.

The findings presented in Fig. 13 suggest a complex relationship between aggregate type, aggregate size, and susceptibility to mass loss when exposed to a 5 % sulfuric acid solution. The data reveals that the relationship between these variables is not uniform, with the magnitude of mass loss varying depending on the specific characteristics of the aggregate. Specifically, when the aggregate type was held constant, the degree of mass loss for basalt aggregate was slightly lower compared to the white limestone (WLS) and brown limestone (BLS) aggregate at a particle size of 10 mm. The mass loss for the B-10, WLS-10, and BLS-10 specimens was approximately 4.8 %, 5.25 %, and 7.2 %, respectively. This suggests that at the smaller aggregate size, the basalt material exhibited a higher resistance to acid-induced degradation compared to the limestone aggregate. However, this trend was reversed when the aggregate size was increased to 14 mm and 20 mm. Under these conditions, the basalt aggregate exhibited a higher mass loss compared to the limestone aggregate. At a size of 14 mm, the mass loss percentages were 8.85 %, 5.3 %, and 7.35 % for the basalt, WLS, and BLS aggregate, respectively. Similarly, at a size of 20 mm, the mass loss was 9.45 %, 7.2 %, and 7.4 % for the basalt, WLS, and BLS aggregate, respectively.

This seemingly contradictory result can be explained by the different underlying degradation mechanisms for siliceous and calcareous aggregates. The acid degradation resistance of basalt aggregate is significantly affected by its chemical composition. As a siliceous aggregate type [41], basalt is characterized by a high silica content (approx. 50 %) and low calcium oxide content (approx. 9 %). This composition renders the aggregate itself relatively inert to sulfuric acid. Therefore, in basalt concrete, the acid primarily attacks the more vulnerable cement paste matrix. The reaction with calcium hydroxide in the paste forms gypsum, a soft, easily removable material, leading to the deterioration of the paste and the dislodging of the inert aggregate particles (Fig. 14a).

This finding aligns with the previous study by Al-Swaidani et al. [39], which demonstrated that during the attack of acidic solution on concrete specimens containing basalt aggregate, only the cement paste was attacked, and the neutralization effect during the acid attack was significantly limited. The mechanism explains the size effect: with larger aggregates (14 and 20 mm), the volume of cement paste per unit volume of concrete is higher (Fig. 15), providing more material for the acid to attack, resulting in greater mass loss. Conversely, with smaller aggregates (10 mm), the paste volume is lower and the aggregate-paste surface area is larger (Fig. 16), leading to a more compact structure where the inert basalt provides better protection to the reduced paste volume, resulting in lower mass loss [42]. This explains the lower mass loss for specimens with smaller aggregate sizes. Fig. 16 shows the relationship between the aggregate-to-cement ratio and the surface area of the cement paste's two components; this relationship diminishes with decreasing cement-to-aggregate ratio. Increasing the quantity of cement paste exposed to the acidic solution is a result of the fact that it is often more porous than coarse aggregate. Porosity, caused by an increase in cement paste, speeds up the rate at which acidic solutions may penetrate concrete and trigger chemical reactions [44].

In contrast, limestone aggregate, being predominantly calcium carbonate ($CaCO_3$) and a low percentage of silica [38,45], follows a different mechanism. It is not inert but acts as a sacrificial material. When exposed to sulfuric acid, the limestone itself reacts to form a dense, solid layer of gypsum ($CaSO_4$) on the surface of the aggregate and the concrete [17].

$$CaCO_3\ (\text{calcium carbonate}) + H_2SO_4 \rightarrow CaSO_4\ (\text{gypsum}) + CO_2\ (\text{carbon dioxide}) + H_2O$$

This newly formed gypsum layer is harder and more adherent than the gypsum formed from the cement paste reaction. It acts as a passivating or protective barrier, slowing down further acid penetration and degradation [20]. This mechanism explains why, at larger aggregate sizes (14 and 20 mm), where the volume of sacrificial limestone is greater, the mass loss is lower than for basalt concrete. The thick, hard-to-remove gypsum layer (Fig. 14b and c) effectively shields the inner concrete. However, this protection is temporary;

Fig. 14. Surface degradation of 15 cm^3 cubic specimens after exposure to sulfuric acid solution: (a) basalt, (b) WLS, and (c) BLS.

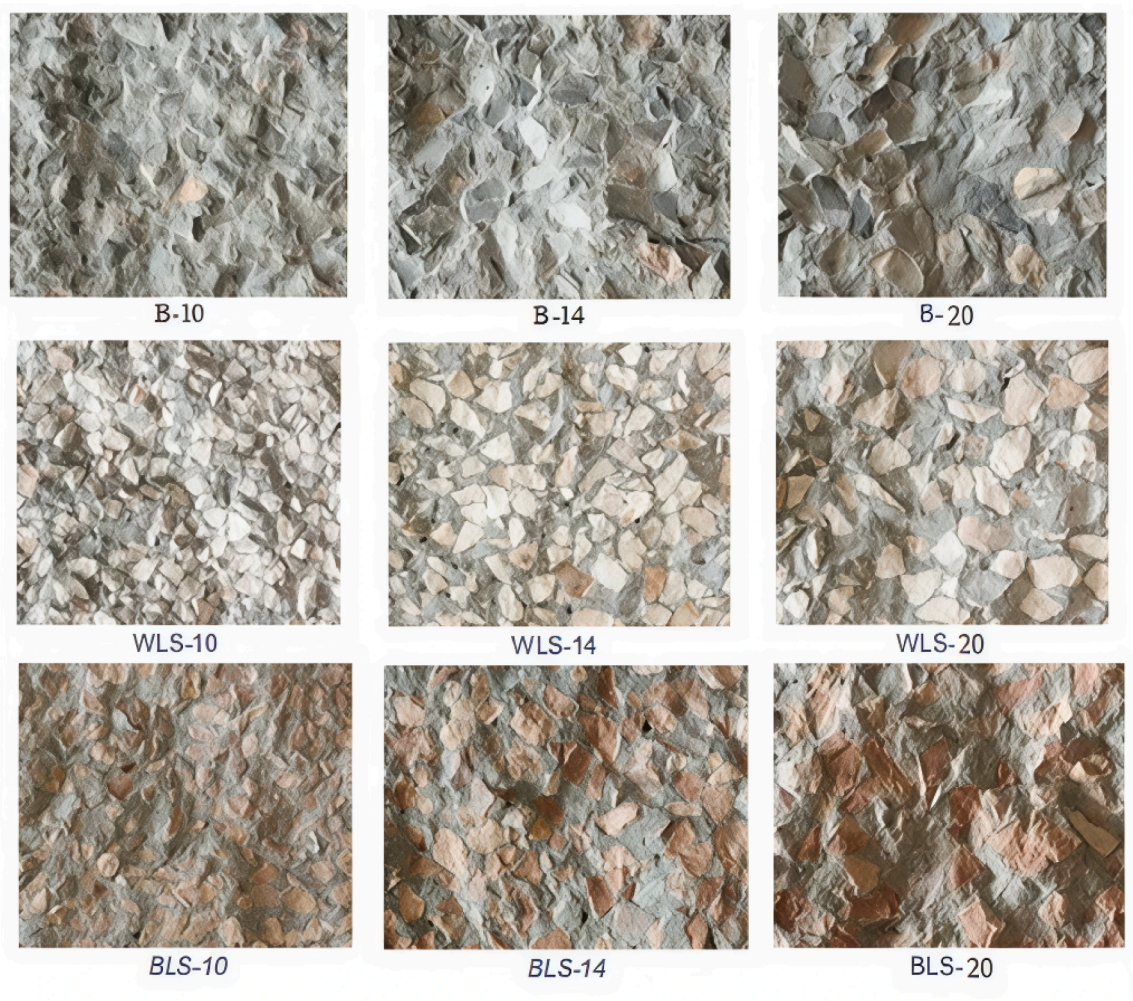

Fig. 15. Volume of cement paste enveloping aggregate particles varies inversely with aggregate size.

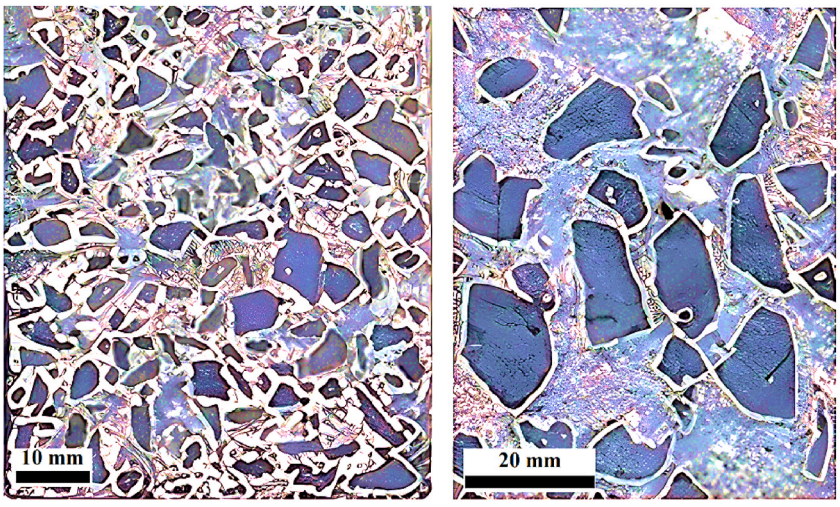

Fig. 16. Reduction in aggregate-cement paste surface area as a function of increased aggregate size.

prolonged exposure would eventually lead to the erosion of this layer and deeper corrosion.

The results presented in this study are consistent with the findings of Ramaswamy and Santhanam [20]. When cement mortar specimens containing limestone (calcareous) fine aggregate and siliceous river sand were exposed to 1 % and 3 % sulfuric acid solutions, the limestone-containing mortar exhibited lower mass loss compared to the specimens with siliceous river sand. This is attributed to the limestone aggregate creating a protective environment due to its solubility in acids, and the dissolved calcium having a preservative effect, shielding the cement paste from acid dissolution. Conversely, the combined effect of the ineffectiveness of the siliceous compounds in basalt aggregate and the lower cement paste content in the 10 mm nominal size specimens led to a reduced mass loss for the basalt aggregate specimens compared to the limestone aggregate ones. Siliceous aggregate is generally inert in acidic environments, primarily due to the very low calcium content in siliceous (basalt) aggregate. During acid attack, the paste will detach, leaving the exposed siliceous aggregate protruding from the concrete surface [20]. However, the increased mass loss observed for the 14 and 20 mm basalt aggregate specimens aligns with the findings of Al-Swaidani et al. [39], who demonstrated that concrete specimens containing basalt aggregate exhibited greater deterioration in terms of mass loss compared to those with dolomitic limestone aggregate.

As mentioned earlier, the brownish color of brown limestone aggregate (BLS) is attributed to the presence of minor impurities such as clay or ferric oxide minerals exceeding 1 % [46]. The existence of these impurities undoubtedly weakens this type of aggregate, rendering it more susceptible to the deleterious effects of sulfuric acid solution compared to the purer white limestone aggregate. Consequently, the weight loss due to sulfuric acid attack is higher for the brown limestone aggregate. Fig. 17a illustrates the extent of erosion and deterioration of the brown limestone aggregate particles exposed to the sulfuric acid solution, exhibiting widespread voids and degradation that affect the majority of the aggregate grains. Fig. 17b demonstrates reduced microstructural density in specimens subjected to sulfuric acid attack. The SEM micrograph reveals degradation of BLS aggregate with associated gypsum deposition. This aggregate's inherently weak microstructure exhibits severe deterioration in both aggregate particles and cement mortar, resulting in significantly higher mass loss compared to WLS aggregate. Generally, the key aggregate-related factors influencing concrete's acid resistance include the mineral composition of the aggregate and the ratio of the total binder volume to the aggregate volume in the concrete mix [47].

3.3.2. *Compressive strength loss*

Fig. 18 presents the compressive strength of specimens containing different aggregate gradations of basalt, white limestone, and brown limestone. Within the aggregate size range investigated in this study, it can be observed that for the same type of aggregate, as the aggregate size increases, the compressive strength decreases. This trend holds true for all the studied aggregate types. This behavior can be attributed to the fact that for the smaller sizes of aggregate, the cement paste is distributed over a larger surface area, effectively covering most of the aggregate particles, allowing for the formation of a denser concrete matrix, which can lead to an increased overall bond area between the adjacent aggregate particles, consequently improving the compressive strength [48]. This finding is corroborated by recent research demonstrating that a reduction in coarse aggregate size leads to a thinner and denser ITZ, which directly enhances the overall mechanical properties of the concrete [49]. Generally, there are several factors that influence the increase and decrease of compressive strength with varying aggregate sizes. Among these factors are the aggregate content in the concrete mix, the shape, texture, and grading of the aggregate, and the concrete grade [50–52]. The findings of this study align with the results obtained by Jin et al. [52], who found that for C30 and C50 concrete grades, the compressive strength decreased significantly with an increase in the coarse aggregate size. Additionally, the study by Mohammed et al. [51] confirmed that when the fine to coarse aggregate volume ratio exceeds 0.45 and the cement content is greater than 350 kg/m^3, the compressive strength decreases with an increase in the maximum aggregate size.

Fig. 18 also illustrates the effect of aggregate type on the 28-day compressive strength of concrete under water curing conditions.

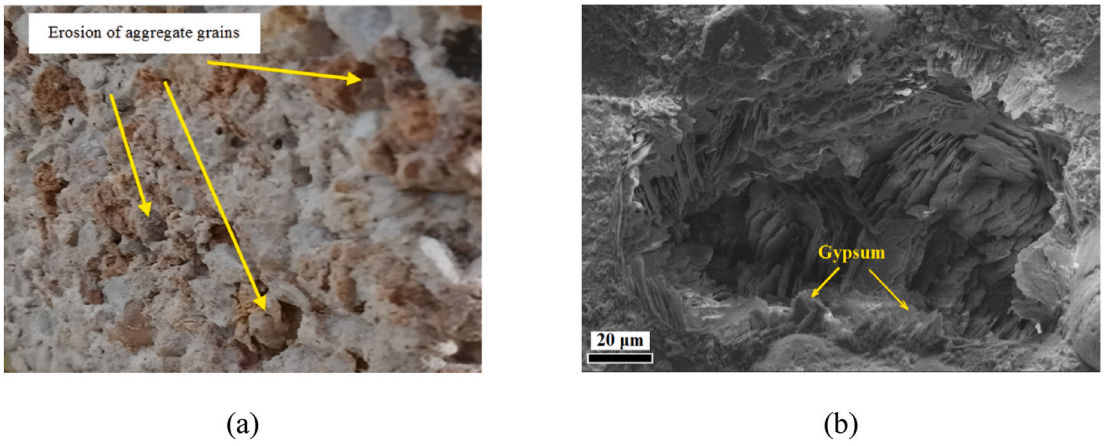

Fig. 17. Degradation of BLS specimen in sulfuric acid solution: (a) surface photomicrograph (overview), and (b) close-up SEM micrograph showing gypsum accumulation.

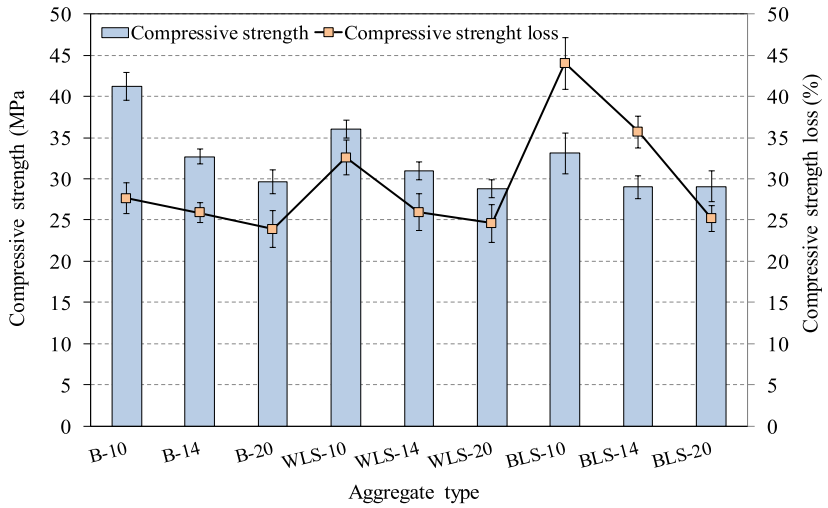

Fig. 18. Compressive strength and its loss after immersion in a sulfuric acid solution as a function of aggregate type and size.

When the aggregate size was 10 mm, the compressive strength of concrete specimens containing basalt aggregate (B-10) was the highest at 41.2 MPa, followed by WLS-10 at 36.04 MPa and BLS-10 at 33 MPa. In the case of the 14 mm aggregate size, a similar trend was observed, with a slight convergence in compressive strengths of B-14, WLS-14, and BLS-14 at 32.7, 31, and 29 MPa, respectively. Notably, at the 20 mm aggregate size, the compressive strengths of B-20, WLS-20, and BLS-20 converged to 29.68, 28.8, and 29.1 MPa, respectively. The convergence of compressive strengths for the 20 mm aggregate size specimens may be attributed to the reduced surface area between the cement paste and aggregate, leading to a more abundant cement paste (Figs. 15 and 16), which contributes significantly to the compressive strength, as the concrete mixtures with the three aggregate types would have similar cement paste volumes [43].

The superior compressive strength of basalt concrete is directly linked to its stronger ITZ compared to limestone concrete. This strength stems from basalt's inherent properties, particularly its rougher surface texture which enhances the bond with the cement paste. In contrast, the weak bond in limestone concrete is caused by a porous surrounding zone, leading to inferior mechanical performance. The inferior mechanical strength of limestone aggregate specimens compared to basalt aggregate mixes can be also attributed to the presence of large calcite crystals in the limestone composition. Calcite crystals exhibit a hexagonal crystalline system with distinct parallel cleavage planes. These planar cleavage surfaces are characterized by relatively low bonding forces and tensile strength compared to the more complex crystalline structure of other materials. Consequently, the existence of these large calcite crystals within limestone transfers these weaker properties to the aggregate as a whole, leading to reduced mechanical durability of the limestone. Furthermore, the influence of limestone on mechanical performance is multifaceted; recent studies have also shown that when used as a fine powder, limestone significantly affects the mechanical properties of the cementitious matrix by altering its microcracking behavior [53]. In contrast, basalt aggregate possesses a more rigid crystalline texture without any weak zones, enhancing the bond strength between the aggregate and the cement paste, which in turn improves the compressive resistance of concrete containing basalt [34]. Furthermore, as previously established in the ITZ characteristics section, the chemical interactions at the aggregate-paste interface differ significantly. XRD analysis showed that the ITZ surrounding limestone aggregate is rich in Tricalcium Silicate (C_3S), whereas the C_3S is notably depleted near the basalt aggregate. This depletion suggests that basalt actively participates in hydration reactions, which indicates a higher chemical activity of basalt compared to limestone aggregate. This heightened reactivity is also evidenced by a higher silicon content detected in the basalt ITZ compared to the limestone ITZ, implying the formation of more calcium silicate hydrates (C-S-H) in the ITZ by the basalt aggregate [54].

Research into using basalt aggregate to improve concrete compressive strength has shown promising results. For instance, Özturan and Çeçen [55] found that basalt-based concrete achieved higher strength than counterparts made with limestone or gravel aggregates. Kishore et al. [56] examined the effect of replacing coarse aggregate with basalt at replacement levels ranging from 0 % to 100 % in 25 % increments. They found that increasing the proportion of basalt aggregate enhanced the compressive strength of the concrete mixtures compared to those containing conventional limestone aggregate. This can be attributed to the fact that basalt is denser, more durable, and less water-absorbent than limestone. In a separate study, Yücel et al. [57] replaced the coarse aggregate with basalt waste at replacement levels of 50 %, 75 %, and 100 %. The results of this study showed that the use of basalt waste led to improvements in the compressive strength of the concrete mixtures. The compressive strength increased by approximately 7 %, 10 %, and 15 % for the WB50, WB75, and WB100 mixtures, respectively, compared to the reference mixture.

Fig. 18 illustrates the compressive strength loss observed for each aggregate type and the effect of varying aggregate size on this loss after subjecting the studied specimens to a 5 % sulfuric acid solution for 30 days. An increase in the rate of strength loss was recorded with decreasing aggregate size. For basalt aggregates with sizes of 10 mm, 14 mm, and 20 mm, the compressive strength loss rates were approximately 27.6 %, 25.9 %, and 23.9 %, respectively. Conversely, the strength loss for white limestone aggregates was 32.6 %,

25.95 %, and 24.6 %, respectively. Meanwhile, the loss for specimens containing brown limestone aggregates was 44.02 %, 35.7 %, and 25.2 %, respectively. Notably, a significant convergence in the percentage of strength loss was observed for specimens containing basalt aggregates compared to those containing limestone aggregates, particularly those with brown limestone aggregates. This difference was most pronounced at an aggregate size of 10 mm.

It was observed that for the same type of aggregate, as the aggregate size decreased, the reduction in compressive strength due to being exposed to a sulfuric acid solution was more pronounced, particularly for concrete mixtures containing brown limestone aggregate. This unexpected phenomenon warrants further investigation, as the typical assumption would be that decreasing aggregate size leads to increased compressive strength. Contrary to this expectation, the data suggests that while decreasing aggregate size may increase the original compressive strength, the loss in strength due to sulfuric acid exposure was greater for mixtures with smaller aggregate sizes. This finding indicates that the effect of sulfuric acid on strength loss was proportional; as the original compressive strength increased, the corresponding loss in compressive strength also increased. Interestingly, the results also imply that the effect of the sulfuric acid on strength loss does not depend heavily on the initial compressive strength. Whether the compressive strength was high or low, it was adversely affected upon exposure to the acidic solution. This effect appears to be influenced by factors beyond just aggregate size, highlighting the need for further research to elucidate the underlying mechanisms.

Based on Fig. 18, when the size of the aggregate is constant, it is clear that basalt aggregates result in less loss in compressive strength compared to other types of aggregate, followed by white limestone and then brown limestone. Specifically, the loss in compressive strength due to exposure to the acidic solution for specimens with aggregate sizes of 10 mm was 27.6 %, 32.6 %, and 44.2 % for specimens B-10, WLS-10, and BLS-10, respectively. These losses were 25.9 %, 25.95 %, and 35.7 % for the same specimens with an aggregate size of 14 mm, and 23.9 %, 24.6 %, and 25.2 % for an aggregate size of 20 mm. The difference in loss of compressive strength is clearly observed when the aggregate size is 10 mm, but this difference decreases as the aggregate size increases, becoming the smallest when the aggregate size is 20 mm. The researchers suggest that this is due to the increased compressive strength of specimens with basalt aggregate as the aggregate size decreases, compared to specimens with WLD and BLS aggregates. This is due to the fact that the surface area between the cement matrix and the aggregate increases, increasing the area of adhesion to the cement paste and reducing the amount of cement matrix exposed to the acidic solution. Furthermore, the deterioration of the cement paste depends on its porosity and the concentration of the acid, as well as the dissolution of the acidic calcium salts (CaX_2) [58]. Additionally, basalt aggregates have a higher resistance to acid due to their mineral composition, making them a more inert filler in acidic environments [20,23]. The similarity in the compressive strength loss between WLS-20, BLS-20, and B-20 may be attributed to the formation of the hard gypsum layer mentioned earlier, which may have covered the surface exposed to the reaction, preventing the continuation of the acid reaction with either the limestone aggregates or the cement mortar [20]. The decrease in the surface area surrounding the basalt aggregate in the B-20 concrete specimens may have reduced the bond between the cement mortar and the aggregate, leading to the observed balance and convergence in the compressive strength loss for WLS-20, BLS-20, and B-20.

The relationship between the initial compressive strength and the subsequent compressive strength loss after immersion in a sulfuric acid solution is depicted in Fig. 19 for concrete mixes with varying aggregate types (basalt, white limestone, and brown limestone) and a constant aggregate size. A positive linear trend is observed, indicating that specimens with higher initial compressive strength tend to exhibit a greater percentage of strength loss. The goodness of fit for this linear relationship is quantified by the coefficient of determination (R^2). For the basalt aggregate specimens, the model shows a strong fit with an R^2 value of 0.8118, suggesting that approximately 81.2 % of the variability in compressive strength loss can be explained by the initial compressive strength. The fit is moderately strong for the white limestone (WLS) and brown limestone (BLS) specimens, with R^2 values of 0.6902 and 0.5998, respectively. These coefficients indicate that the initial compressive strength is a significant predictor of acid-induced strength loss, particularly for the concrete made with basalt aggregate. Based on these findings, the initial compressive strength can be used as an approximate predictor for the compressive strength loss due to sulfuric acid exposure. However, it is important to acknowledge that this relationship may be influenced by other variables. To validate and expand upon this result, further studies are necessary to examine the effects of varying parameters, such as the concentration of the sulfuric acid solution, different aggregate sizes, and the duration of immersion.

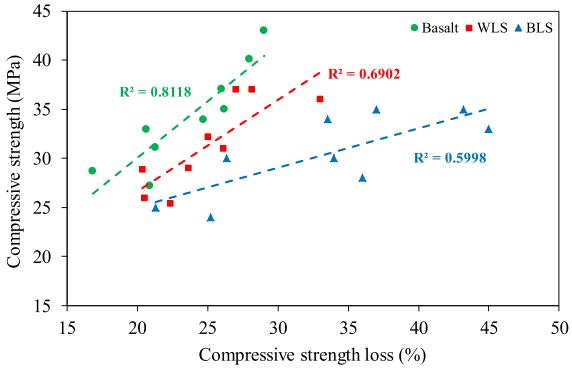

Fig. 19. Statistical correlation of compressive strength and acid-induced losses.

3.3.3. Visual assessment

The application of phenolphthalein solution to the cross-sectional surfaces of specimens exposed to sulfuric acid solution revealed the presence of pink-colored regions, indicating a pH level greater than 8.5 in those areas. Conversely, the colorless regions suggest a pH level below 8.0 [30]. A visual examination of the cross-sectional appearance of the specimens containing the studied aggregates, which were sprayed with phenolphthalein solution after being exposed to a 5 % sulfuric acid solution for 30 days prior to sectioning, is shown in Fig. 20. Upon application of the phenolphthalein solution, no colorless zones were observed on the cross-sectional surfaces of any specimen. Instead, a uniform light pink color was noted, indicating that the acid had not penetrated deeply enough to neutralize the concrete's alkalinity to a pH below 8.0.

The visual assessment indicated that the acid attack was primarily confined to the surface of the specimens, without significant deep penetration. The primary manifestation of this surface-level deterioration was the formation of a gypsum layer, which was clearly observable on the specimens containing limestone aggregates. The thickness of this layer varied with aggregate type, measuring approximately 10 mm for white limestone and 5 mm for brown limestone specimens (Fig. 21a and b). In contrast, this layer was less discernible on the basalt aggregate specimens (Fig. 21c). The lack of deep acid penetration into the concrete specimens containing limestone aggregates can be attributed to the insulating environment created by the solubility of limestone aggregates in acids. The dissolved calcium, therefore, has a protective effect, shielding the cement paste from further deterioration. In the case of basalt, the chemical inertness of its siliceous compounds limited the reaction, as siliceous aggregates are considered resistant to acidic environments due to their very low calcium content [20].

Although the visual manifestations of damage were similar across specimens (i.e., limited to the surface), this criterion alone is insufficient to assess the relative performance comprehensively. A full evaluation requires the integration of physical, chemical, and mechanical test results, as well as detailed microstructural examinations, to provide a complete understanding of the material's performance.

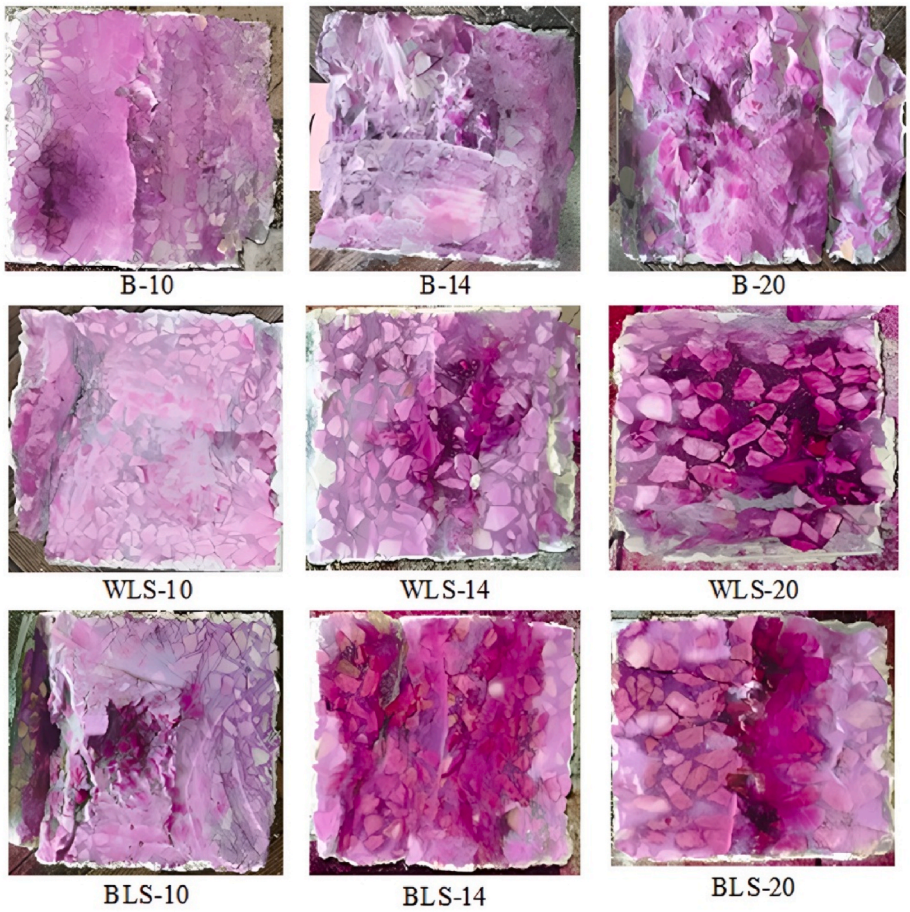

Fig. 20. Visual inspection of aggregate-containing specimens sprayed with phenolphthalein.

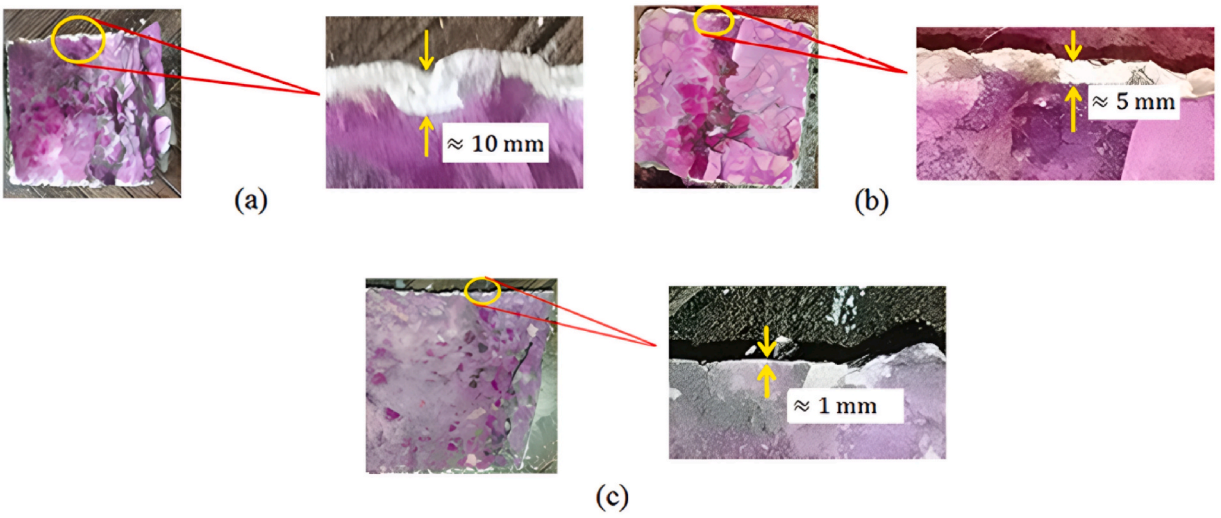

Fig. 21. Gypsum layer thickness due to acid reaction of (a) WLS, (b) BLS, and (c) basalt aggregate.

3.4. Water permeability evaluation

3.4.1. Depth of water penetration

The depth of water penetration into concrete is an indicator of its permeability, or impermeability. If the depth of water penetration is less than 50 mm, the concrete is classified as impermeable. Furthermore, if the penetration depth is less than 30 mm, the concrete is considered impermeable under aggressive conditions [9]. Table 4 presents the measured water penetration depths for concrete specimens containing the investigated aggregate. Based on the data presented in the table, it is evident that the type and size of aggregate significantly affect the water penetration depth. When the aggregate size is constant, specimens containing basalt aggregate exhibited a superior ability to resist water penetration compared to other aggregate types. Moreover, the size of the aggregate plays a crucial role in minimizing water ingress within the concrete specimens. When the aggregate type is consistent, the water penetration depth is considerably lower in cases with smaller aggregate sizes. Furthermore, according to the results presented in Table 4, all of the concrete specimens used in this study are considered impermeable to water. However, they also exhibit resistance against aggressive conditions that concrete typically encounters due to permeability factors, except for the specimens containing brown limestone aggregate with a size of 20 mm. These specimens might have a reduced capacity to withstand the intrusion of harmful substances and materials due to the water penetration depth ranging between 27 and 33 mm. This relationship is further illustrated in Fig. 22, which highlights the variation in water penetration depth among the specimens based on the type and size of the aggregate.

3.4.2. Permeability coefficient

Fig. 23 illustrates the effect of aggregate size on the permeability coefficient of concrete specimens for various types of aggregate. Specifically, it is observed that a decrease in aggregate size in the concrete mixture corresponds to a decrease in the permeability coefficient. For mixtures containing basalt aggregate, this reduction is approximately 75 % when the aggregate size decreases from 20 mm to 10 mm. For concrete mixtures with white limestone aggregate, the reduction is approximately 85 %, while for those with brown limestone aggregate, the reduction is about 76 %.

It is well established that concrete made with well-graded aggregate tends to have a higher density compared to concrete made with poorly-graded aggregate. As mentioned previously, in the case of smaller aggregate sizes, the aggregate particles are in closer proximity, providing a larger surface area and a more uniform distribution of the cement paste between the aggregate particles, leading to improved density. The smaller particles also fill the voids between the larger aggregate particles. Consequently, the contact between the aggregate particles is increased, and the effective porosity is reduced [59]. Conversely, with larger aggregate sizes, the voids and air content increase, leading to increased air permeability and, hence, increased water permeability [60]. This is due to the increased porosity in the interfacial transition zone (ITZ) between the cement paste and the aggregate particles, which can be attributed to a

Table 4
Depth of water penetration into specimens (mm).

Agg. Size (mm) Agg. Type	10	14	20
Basalt	9 ± 2	13 ± 2	23 ± 2
White limestone	13 ± 2	16 ± 2	29 ± 2
Brown limestone	14 ± 2	21 ± 3	30 ± 3

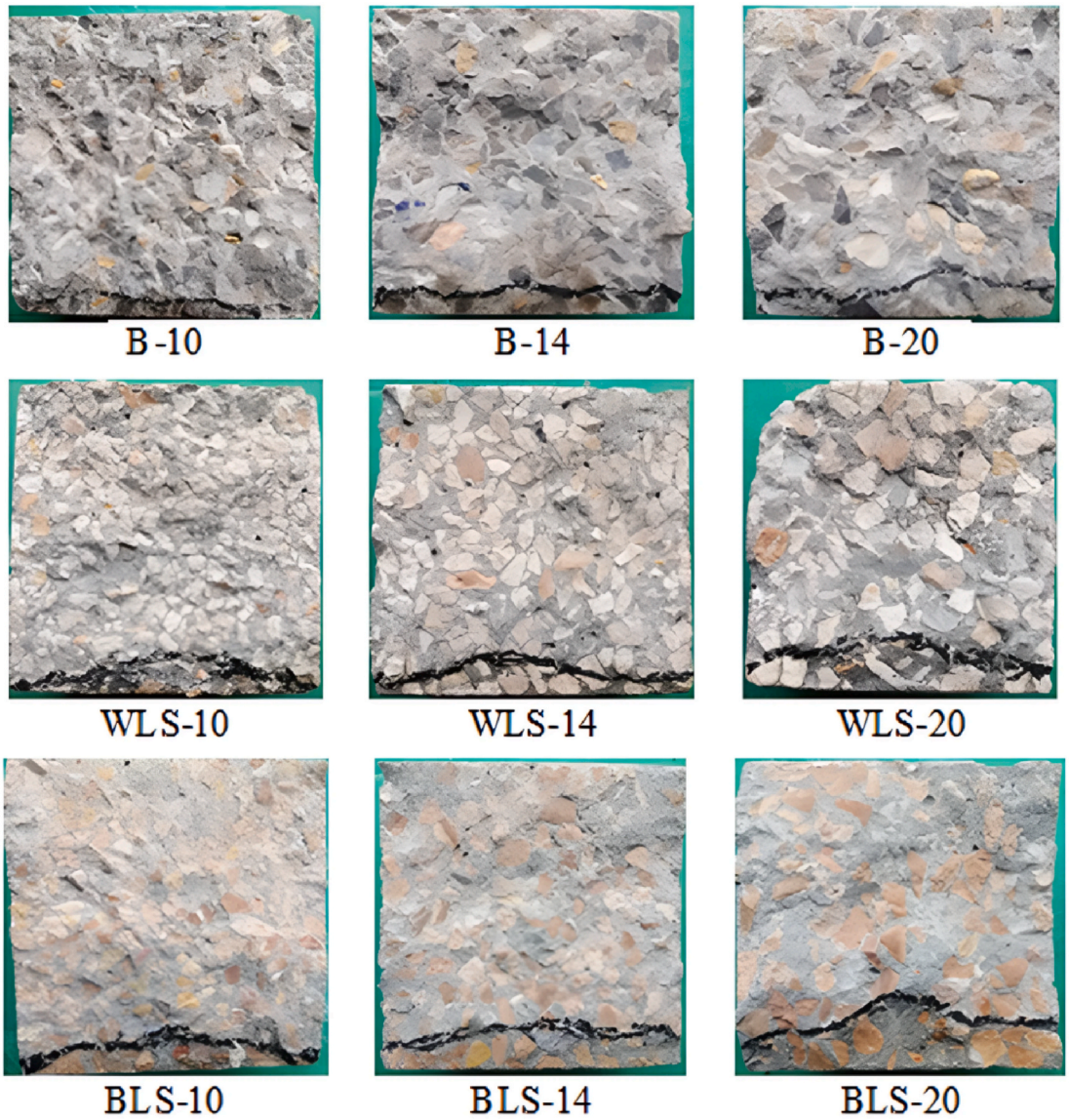

Fig. 22. Depth of water penetration varies aggregate type and size.

reduction in the tortuosity of the flow path, tending to increase both air and water permeability, as well as the increased likelihood of water ponding beneath the coarse aggregates [61].

Overall, the effect of aggregate size on reducing permeability, independent of the role of the cementitious matrix, is that the addition of smaller aggregate to concrete results in an improved pore size distribution. As the amount of smaller aggregate in the concrete increases, the proportion of large-sized pores decreases, and the effective pore size that significantly contributes to water permeability also decreases [62]. The results of this study align with the findings of Yogesh et al. [63], who demonstrated that the concrete permeability was significantly lower when using a gradation of 4.75–22.5 mm compared to a gradation of 16–22.5 mm. These results also support the findings of Yang et al. [64], who showed that increasing the aggregate size in the cementitious matrix significantly affects the permeability and porosity, with an increase in aggregate size resulting in a more porous internal structure and an increase in permeability.

Analysis of aggregate type effects revealed that basalt aggregate conferred superior impermeability to concrete mixtures versus white limestone aggregate, exhibiting the lowest permeability coefficients for all particle sizes investigated (10, 14, and 20 mm). The percentage reduction in permeability coefficient for concrete mixes with basalt aggregate was approximately 55 % and 75 % compared to white limestone (WLS) and brown limestone (BLS) aggregate, respectively, at the 10 mm size. This reduction was 47 % and 84 % at the 14 mm size, and 48 % and 75 % at the 20 mm size. The decrease in permeability coefficient for white limestone (WLS) aggregate mixes compared to brown limestone (BLS) mixes was 43 % at the 10 mm aggregate size, 70 % at the 14 mm size, and 52 % at the 20 mm

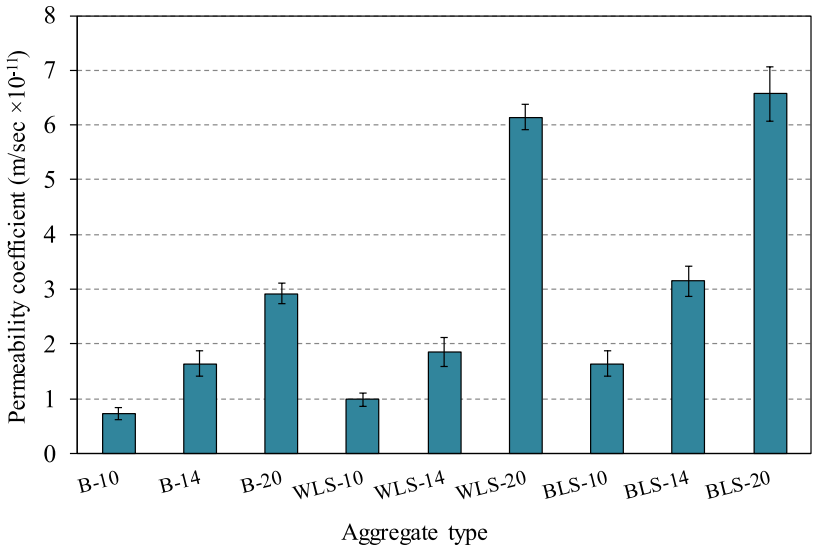

Fig. 23. Effect of aggregate type and size variations on permeability coefficient.

size. These results demonstrate that the type and mineralogical composition of the aggregate play a significant role in influencing the water permeability of concrete. The superior performance of basalt concrete is a direct consequence of the refined ITZ discussed earlier. The combination of strong mechanical interlocking from its rough texture and chemical densification from the pozzolanic reaction creates a less porous and more tortuous pathway for water ingress, significantly reducing permeability [35,36].

Generally, the water permeability of concrete depends on several factors, such as the water-to-cement ratio, the number and size of pores in the cement paste surrounding the aggregate [65], as well as the grading of the aggregate, their water absorption capacity, void content, and discontinuous pore structure of the aggregate [66,67]. Toplicic-Curcic et al. [65] found that the effect of aggregate type on water permeability depends largely on the water-to-cement ratio. The superior performance of basalt aggregate in reducing water penetration is observed at a water-to-cement ratio of 0.45, compared to other mixes containing limestone, diabase, and andesite. However, this advantage is reversed at a water-to-cement ratio of 0.65. Thus, the effectiveness of basalt in limiting water penetration is more pronounced when the matrix porosity resulting from low water-to-cement ratios is reduced. Moreover, permeability is significantly affected by the porosity and void content of the aggregate, as well as the water absorption rate [68]. Porosity and water absorption are indicators of the presence of pores or voids in concrete. Therefore, an increase in these factors can lead to an increase in water permeability [69]. In terms of the mechanical properties of the aggregate, it is found that basalt aggregate has a lower water absorption rate compared to limestone aggregate, with water absorption rates of 0.58 %, 1.12 %, and 1.28 % for basalt, WLS, and BLS, respectively. This suggests that the lower permeability of basalt-based concrete mixtures compared to limestone-based concrete mixtures can be attributed to the lower water absorption rate and lower porosity of basalt aggregate [70]. The results of this study are consistent with the findings of Al-Baijat [71], who observed that the average water penetration depth for three tests on specimens of concrete with basalt and limestone aggregate was 18 mm and 25 mm, respectively, indicating that permeability is inversely proportional to the basalt content in the concrete mixture. This is because basalt is denser than limestone, and replacing limestone with basalt in the concrete mixture increases the mixture's density and reduces its permeability. However, the permeability values for all mixtures in this study still fall within the acceptable range for conventional concrete, which is (10^{-11} – 10^{-12} m/s) [72].

Previous studies have demonstrated that the interfacial transition zone (ITZ) between the cement paste and aggregate is the weakest region in the concrete composite [67,73]. The mineral composition and water absorption rate of the aggregate is crucial factors that directly influence the bond strength between the aggregate and the cement paste. Chemical reactions between certain types of rocks and the cement paste can lead to a decrease in bond strength rather than an increase. This is particularly true for the interaction between limestone and cement paste. As previously discussed in this paper, the chemical reaction between limestone aggregate and the cement paste leads to the formation of a highly porous interfacial transition zone (ITZ), a phenomenon attributed to the release of carbon dioxide gas. However, this porous transition zone leads to a reduction in the bond strength between the components, consequently decreasing the strength and increasing the permeability of the concrete [35]. Furthermore, through their studies of the surface interaction between cement paste and various types of aggregate, Kong and Du [36] have shown that the volume content of large pores in the ITZ of basalt is less than that of limestone, specifically for pores ranging from 100 to 1000 nm. For instance, when compared to the pore size distribution around limestone, the content of large pores in the specimen around basalt in the range of 100–1000 nm is reduced by 27 %. This observation can be attributed to the chemical interaction between the aggregate and the cement paste, which increases hydrate production, leading to the filling of pores and a denser structure around basalt compared to limestone. On the other hand, more porous aggregates continue to absorb water from the cement paste even after casting. As water absorption continues due to its hairy nature, the air replaced by the water accumulates in small bubbles on the interface between the cement paste

and the aggregate (ITZ). This process continues until the cementitious matrix solidifies. The amount of air that can be expelled after casting depends on the aggregate's ability to absorb water. The air bubbles present at the ITZ interface tend to reduce the contact area of the cement paste, resulting in decreased strength and increased permeability [74]. This is expected for limestone, which has higher water absorption compared to basalt. As previously mentioned, basalt has a crystalline texture with a higher surface hardness compared to other types of aggregate, which is characterized by the absence of weak areas in its composition [35]. These properties contribute to increased bonding strength between basalt aggregate particles and cement paste, leading to lower permeability in concrete made with this type of aggregate.

The relationship between compressive strength and permeability coefficient for the different aggregate types is illustrated in Fig. 24. A clear inverse relationship is observed between compressive strength and the permeability coefficient for all tested concrete mixtures, as indicated by the negative slope of the trend lines. The strength of this linear correlation is quantified by the coefficient of determination (R^2), which was calculated for each aggregate type. All R^2 values were high, indicating a strong correlation. Specifically, the coefficients of determination (R^2) were recorded as 0.8624 for basalt, 0.8417 for white limestone (WLS), and 0.8279 for brown limestone (BLS) aggregate specimens. The R^2 value for the basalt aggregate specimens is the highest, which is consistent with the superior performance of basalt aggregate specimens in terms of both compressive strength and permeability, reflecting the strong statistical link between these two properties. Generally, within the scope and limits of this study, this strong correlation suggests that the relationship can be used to predict the permeability coefficient from the compressive strength, and vice versa. The physical reason for this inverse relationship is that a reduction in permeability is associated with decreased pore connectivity and porosity. This leads to a denser, less porous microstructure, which in turn results in higher compressive strength [75]. Conversely, the presence of interconnected pores and voids weakens the concrete's internal structure, making it more susceptible to failure under load and thus resulting in lower compressive strength [76]. Furthermore, since the cement paste was a constant variable for all the concrete mixtures studied, the type of aggregate plays a crucial role in this relationship. The strength of the relationship between permeability and compressive strength is influenced by the aggregate type. Aggregates with lower intrinsic permeability, higher density, and lower water absorption will contribute to a stronger concrete matrix, enhancing compressive strength. This is evident from the superior performance of concrete mixtures containing basalt aggregate, followed by white limestone aggregate.

4. Conclusion

This study systematically evaluated the combined influence of aggregate type (basalt, white limestone, brown limestone) and size (10, 14, 20 mm) on concrete durability. The research focused on assessing acid resistance and water permeability, linking the performance outcomes to the microstructural and mechanical properties of the aggregate-cement interfacial transition zone. According to the series of experiments, the following conclusions are obtained.

1. A key contribution of this study is demonstrating that the nature of aggregate roughness, not just its magnitude, is critical for bond strength. Fractured surfaces are superior to sawn ones, but basalt's high-peak topography provides better mechanical interlocking than limestone's valley-dominated texture. This physical advantage, combined with basalt's pozzolanic reactivity which consumes weak CH to form dense C-S-H, results in a significantly stronger and less porous ITZ compared to limestone.
2. This work elucidates the competing mechanisms of acid attack based on aggregate type. For siliceous basalt, degradation is governed by the erosion of the vulnerable cement paste, making smaller aggregate sizes (with less paste) more resistant. For calcareous limestone, the aggregate acts as a sacrificial buffer, forming a protective gypsum layer that provides temporary resistance, an effect more pronounced with larger aggregate volumes.
3. Increasing aggregate size leads to a decrease in the compressive strength of concrete, a trend observed across all aggregate types. Concrete made with 10 mm basalt aggregate achieved the highest compressive strength, as its superior physical properties and stronger interfacial bond consistently yield better results than limestone aggregates. Following sulfuric acid exposure, basalt concrete demonstrated the least compressive strength reduction compared to limestone varieties. Basalt's superior acid resistance,

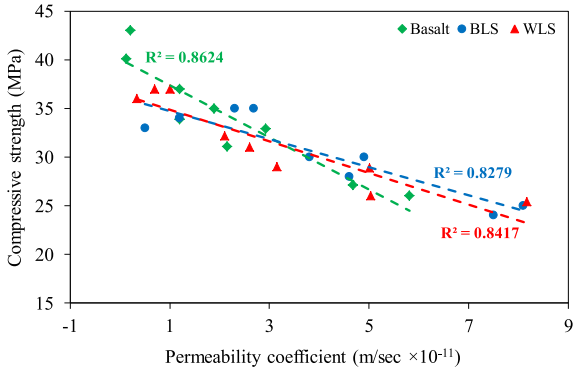

Fig. 24. Statistical correlation of compressive strength and permeability coefficient.

especially with smaller aggregates, is attributed to its inert siliceous composition and an increased cement-aggregate surface area, which enhances adhesion and protects the more vulnerable cement mortar.

4. This study confirms that the superior ITZ of basalt concrete directly translates to enhanced durability. Basalt concrete exhibited the lowest water permeability due to its refined, denser microstructure, which creates a more tortuous path for water penetration. Permeability decreased significantly with smaller aggregate sizes for all types, highlighting the importance of particle packing.
5. A strong inverse correlation was established between compressive strength and permeability, with basalt concrete showing the most significant relationship. This highlights that basalt aggregate is highly effective for producing concrete that simultaneously achieves high compressive strength and low permeability, which are critical for ensuring long-term durability in aggressive environments.

While this study successfully linked ITZ characteristics to concrete performance using qualitative SEM and semi-quantitative XRD analysis, it is recommended that future research employ more advanced quantitative methods to build upon these findings. For instance, future investigations should leverage advanced imaging techniques to provide a multi-scale quantitative assessment. This includes using 2D quantitative image analysis to determine specific ITZ indices such as porosity and pore-size distribution, complemented by 3D techniques like X-ray Computed Tomography (X-CT) to accurately quantify aggregate surface roughness and morphology. Such an approach would allow for establishing direct correlations between aggregate topography and the interfacial structure. Concurrently, the application of quantitative XRD techniques, such as the Rietveld refinement method, would enable the precise determination of the absolute contents of hydration products (e.g., CH) and unhydrated phases. This would move beyond the relative comparisons made in this work and provide a more rigorous, data-driven understanding of the physical and chemical mechanisms governing the aggregate-paste bond and its direct impact on concrete performance.

CRediT authorship contribution statement

Nurdeen M. Altwair: Writing – review & editing, Writing – original draft, Software, Methodology, Investigation, Formal analysis, Data curation, Conceptualization. **Ashraf M. Al-Kilani:** Writing – original draft, Supervision, Resources, Methodology, Funding acquisition, Data curation. **Mustafa M. Al-Tayeb:** Writing – review & editing, Resources, Methodology, Funding acquisition. **Ramadhansyah Putra Jaya:** Writing – review & editing, Software, Methodology.

Declaration of competing interest

The authors declare that they have no known competing financial interests or personal relationships that could have appeared to influence the work reported in this paper.

Data availability

The data that has been used is confidential.

References

[1] H. Beshr, A.A. Almusallam, M. Maslehuddin, Effect of coarse aggregate quality on the mechanical properties of high strength concrete, Constr. Build. Mater. 17 (2003) 97–103, https://doi.org/10.1016/s0950-0618(02)00097-1.
[2] T. Yao, Y. Wang, M. Li, W. Zhang, S. Luo, Q. Tian, J. Chen, Recycling coal gasification slag to produce eco-friendly ultra-high performance concrete: working properties, mechanical properties and microstructure, Cem. Concr. Compos. 164 (2025) 106260, https://doi.org/10.1016/j.cemconcomp.2025.106260.
[3] F. Patowary, R.A. Mahmood, Effect of local coarse aggregate type on concrete mechanical properties in Bangladesh, Int. J. Eng. Adv. Tech. 11 (2022) 104–107, https://doi.org/10.35940/ijeat.d3490.0411422.
[4] I.H.M. Albarwary, Z.N.S. Aldoski, L.K. Askar, Effect of aggregate maximum size upon compressive strength of concrete, J. Dohuk Univ. 20 (2017) 790–797, https://doi.org/10.26682/sjuod.2017.20.1.67.
[5] D. Alfonso, M. Dugarte, J. Carrillo, C.A. Arteta, Effect of aggregate type on the elastic modulus and compressive behavior of concrete: a case study in Colombia, Constr. Build. Mater. 411 (2024) 134131, https://doi.org/10.1016/j.conbuildmat.2023.134131.
[6] X. Li, Q. Xu, S. Chen, An experimental and numerical study on water permeability of concrete, Constr. Build. Mater. 105 (2016) 503–510, https://doi.org/10.1016/j.conbuildmat.2015.12.184.
[7] R. Chini, C. Muszynski, K. Hicks, Determination of Acceptance Permeability Characterestics for performance- Related Specifications for Portlant Cement Concrete, Report Submitted to Florida Department of Transportation, USA, 2003.
[8] M. Hoseini, V. Bindiganavile, N. Banthia, The effect of mechanical stress on permeability of concrete: a review, Cem. Concr. Compos. 31 (2009) 213–220, https://doi.org/10.1016/j.cemconcomp.2009.02.003.
[9] A. Neville, Properties of Concrete, fifth ed., Pearson Education Limited, London, 2011.
[10] S. Ahmad, A.K. Azad, K.F. Loughlin, Effect of the key mixture parameters on tortuosity and permeability of concrete, J. Adv. Concr. Technol. 10 (2012) 86–94, https://doi.org/10.3151/jact.10.86.
[11] P. Soongswang, M. Tia, D. Bloomquist, Factors affecting the strength and permeability of oncrete made with porous limestone, ACI Mater. J. 4 (1991) 400–406, https://doi.org/10.14359/1915.
[12] H.R. Samaha, K.C. Hover, Influence of microcracking on the mass transport properties of concrete, ACI Mater. J. 89 (1992) 416–424, https://doi.org/10.14359/2585.
[13] R. Mills, Gas and Water Permeability of Concrete for Reactor Building – Small Specimens, INFO-0188-1, Atomic Energy Control Board and University of Toronto, 1987.
[14] S. Larreur-Cayol, A. Bertron, G. Escadeillas, Degradation of cement-based materials by various organic acids in agro-industrial waste-waters, Cem. Concr. Res. 41 (2011) 882–892, https://doi.org/10.1016/j.cemconres.2011.04.007.

[15] S.A. Hasan, M. Billah, M. Billah, H. Chowdhury, R. Amin, M.R. Parven, M. Islam, S. Hasan, Chemical attack on concrete in wastewater treatment plant: a review, Aust. J. Eng. . Innovative Technol. (2023) 192–205, https://doi.org/10.34104/ajeit.023.01920205.
[16] J. Xiao, Z. Xu, Y. Murong, L. Wang, B. Lei, L. Chu, H. Jiang, W. Qu, Effect of chemical composition of fine aggregate on the frictional behavior of concrete–soil interface under sulfuric acid environment, Fractal. Fractional. 6 (2021) 22, https://doi.org/10.3390/fractalfract6010022.
[17] J. Xiao, W. Qu, W. Li, P. Zhu, Investigation on effect of aggregate on three non-destructive testing properties of concrete subjected to sulfuric acid attack, Constr. Build. Mater. 115 (2016) 486–495, https://doi.org/10.1016/j.conbuildmat.2016.04.017.
[18] N. De Belie, J. Monteny, A. Beeldens, E. Vincke, D. Van Gemert, W. Verstraete, Experimental research and prediction of the effect of chemical and biogenic sulfuric acid on different types of commercially produced concrete sewer pipes, Cem. Concr. Res. 34 (2004) 2223–2236, https://doi.org/10.1016/j.cemconres.2004.02.015.
[19] T. Dyer, Concrete Durability, first ed., Taylor & Francis Group, London, 2014 https://doi.org/10.1201/b16793.
[20] K.P. Ramaswamy, M. Santhanam, Influence of mineralogical nature of aggregates on acid resistance of mortar, in: Proceedings of Sixth International Conference on Durability of Concrete Structures, University of Leeds, United Kingdom, 2018, pp. 256–266. United Kingdom.
[21] Z.-T. Chang, X.-J. Song, R. Munn, M. Marosszeky, Using limestone aggregates and different cements for enhancing resistance of concrete to sulphuric acid attack, Cem. Concr. Res. 35 (2005) 1486–1494, https://doi.org/10.1016/j.cemconres.2005.03.006.
[22] T.A. Aiken, L. Gu, J. Kwasny, G.F. Huseien, D. McPolin, W. Sha, Acid resistance of alkali-activated binders: a review of performance, mechanisms of deterioration and testing procedures, Constr. Build. Mater. 342 (2022) 128057, https://doi.org/10.1016/j.conbuildmat.2022.128057.
[23] C.M. Ninan, K.P. Ramaswamy, R. Sajeeb, Influence of concrete mixture composition on acid resistance of concrete: a review, AIJR Proceedings (2021), https://doi.org/10.21467/proceedings.112.53.
[24] A. Pandey, B. Kumar, Investigation on the effects of acidic environment and accelerated carbonation on concrete admixed with rice straw ash and microsilica, J. Build. Eng. 29 (2020) 101125, https://doi.org/10.1016/j.jobe.2019.101125.
[25] S. Miyamoto, H. Minagawa, M. Hisada, Deterioration rate of hardened cement caused by high concentrated mixed acid attack, Constr. Build. Mater. 67 (2014) 47–54, https://doi.org/10.1016/j.conbuildmat.2013.11.008.
[26] B. Pather, S.O. Ekolu, H. Quainoo, Acid-resistance behaviors of natural aggregates, J. Mater. Civ. Eng. 34 (2022), https://doi.org/10.1061/(asce)mt.1943-5533.0004289.
[27] M. Jebli, F. Jamin, E. Malachanne, E. Garcia-Diaz, E. Youssoufi, Experimental characterization of mechanical properties of the cement-aggregate interface in concrete, Constr. Build. Mater. 161 (2018) 16–25, https://doi.org/10.1016/j.conbuildmat.2017.11.100.
[28] G.C. Lee, Y. Kim, S.Y. Seo, H.D. Yun, S. Hong, Sulfuric acid resistance of cnt-cementitious composites, Appl. Sci. 11 (2021) 2226, https://doi.org/10.3390/app11052226.
[29] M.T. Bassuoni, M. Nehdi, M. Amin, Self-compacting concrete: using limestone to resist sulfuric acid, proceedings of the institution of civil engineers. Constr, Mater 160 (2007) 113–123, https://doi.org/10.1680/coma.2007.160.3.113.
[30] I. Fernandes, M. Pericão, P. Hagelia, F. Noronha, M.A. Ribeiro, J. Maia, Identification of acid attack on concrete of a sewage system, Mater. Struct. 45 (2011) 337–350, https://doi.org/10.1617/s11527-011-9769-y.
[31] S.I. Ahmad, MdS. Rahman, MdS. Alam, Water permeability properties of concrete made from recycled brick concrete as coarse aggregate, IOP conference series, Mater. Sci. Eng. 809 (2020) 012015, https://doi.org/10.1088/1757-899x/809/1/012015.
[32] J. An, S. Kim, B. Nam, S. Durham, Effect of aggregate mineralogy and concrete microstructure on thermal expansion and strength properties of concrete, Applied Sciences 7 (2017) 1307, https://doi.org/10.3390/app7121307.
[33] Z. Jiang, Y. Mao, D. Jiao, X. Hu, C. Shi, Insights into the role of aggregate shape in enhancing rheology and reducing cement usage in concrete mixture design, J. Build. Eng. (2025) 112073, https://doi.org/10.1016/j.jobe.2025.112073.
[34] W.A. Tasong, C.J. Lynsdale, J.C. Cripps, Aggregate-cement paste interface. ii: influence of aggregate physical properties, Cem. Concr. Res. 28 (1998) 1453–1465, https://doi.org/10.1016/s0008-8846(98)00126-4.
[35] W.A. Tasong, C.J. Lynsdale, J.C. Cripps, Aggregate-cement paste interface Part I. Influence of aggregate geochemistry, Cem. Concr. Res. 29 (1999) 1019–1025, https://doi.org/10.1016/s0008-8846(99)00086-1.
[36] L. Kong, Y. Du, Interfacial interaction of aggregate-cement paste in concrete, J. Wuhan Univ. Technol. 30 (2015) 117–121, https://doi.org/10.1007/s11595-015-1111-z.
[37] F. Bellmann, B. Möser, J. Stark, Influence of sulfate solution concentration on the formation of gypsum in sulfate resistance test specimen, Cem. Concr. Res. 36 (2006) 358–363, https://doi.org/10.1016/j.cemconres.2005.04.006.
[38] Z. Makhloufi, E.H. Kadri, M. Bouhicha, A. Benaissa, Resistance of limestone mortars with Quaternary binders to sulfuric acid solution, Constr. Build. Mater. 26 (2012) 497–504, https://doi.org/10.1016/j.conbuildmat.2011.06.050.
[39] N.A.M. Al-Swaidani, N.M.K. Baddoura, N.S.D. Aliyan, N.W. Choeb, Acid resistance, water permeability and chloride penetrability of concrete containing crushed basalt as aggregates, J. Mater. Sci. Eng. 5 (2015), https://doi.org/10.17265/2161-6213/2015.7-8.005.
[40] J. Monteny, E. Vincke, A. Beeldens, N. De Belie, L. Taerwe, D. Van Gemert, W. Verstraete, Chemical, microbiological, and in situ test methods for biogenic sulfuric acid corrosion of concrete, Cem. Concr. Res. 30 (2000) 623–634, https://doi.org/10.1016/s0008-8846(00)00219-2.
[41] S. Yang, H. Chen, The Early Permian Tarim Large Igneous Province in Northwest China, Elsevier, 2018.
[42] M. Harini, G. Shaalini, G. Dhinakaran, Effect of size and type of fine aggregates on flowability of mortar, KSCE J. Civ. Eng. 16 (2011) 163–168, https://doi.org/10.1007/s12205-012-1283-4.
[43] M.T. Uddin, A.H. Mahmood, MdR.I. Kamal, S.M. Yashin, Z.U.A. Zihan, Effects of maximum size of brick aggregate on properties of concrete, Constr. Build. Mater. 134 (2017) 713–726, https://doi.org/10.1016/j.conbuildmat.2016.12.164.
[44] P.C. Kreijger, The skin of concrete composition and properties, matér, Constr. Met. (CTICM) 17 (1984) 275–283, https://doi.org/10.1007/bf02479083.
[45] C. Aquino, M. Inoue, H. Miura, M. Mizuta, T. Okamoto, The effects of limestone aggregate on concrete properties, Constr. Build. Mater. 24 (2010) 2363–2368, https://doi.org/10.1016/j.conbuildmat.2010.05.008.
[46] M. Eriksson, K. Sandström, M. Carlborg, M. Broström, Impact of limestone surface impurities on quicklime product quality, Miner. 14 (2024) 244, https://doi.org/10.3390/min14030244.
[47] K. Ramaswamy, A. Bertron, M. Santhanam, Additional insights on the influencing factors and mechanism of degradation due to acid attack: special case of acids forming soluble salts, in: Proceedings of International Conference on Advances in Construction Materials and Systems (ICACMS), 4, 2017, pp. 279–290. Chennai.
[48] G. Xu, W. Shen, X. Huo, Z. Yang, J. Wang, W. Zhang, X. Ji, Investigation on the properties of porous concrete as road base material, Constr. Build. Mater. 158 (2018) 141–148, https://doi.org/10.1016/j.conbuildmat.2017.09.151.
[49] Y. Wang, W. Zhang, J. Wang, R. Huang, G. Lou, S. Luo, Effects of coarse aggregate size on thickness and micro-properties of ITZ and the mechanical properties of concrete, Cem. Concr. Compos. 154 (2024) 105777, https://doi.org/10.1016/j.cemconcomp.2024.105777.
[50] G.T. Abegaz, I. Khan, A.M. Legese, Investigating the effects of coarse aggregate physical properties on strength of c-25 concrete, Am. J. Eng. Technol. Manage. 5 (2020) 84, https://doi.org/10.11648/j.ajetm.20200505.12.
[51] T.U. Mohammed, A.H. Mahmood, A. Sakib, F.A. Khan, S.I. Sopnil, Fresh and hardened properties of brick aggregate concrete with maximum aggregate sizes of 10 mm to 75 mm, Constr. Mater. 3 (2023) 337–353, https://doi.org/10.3390/constrmater3040022.
[52] L. Jin, W. Yu, D. Li, X. Du, Numerical and theoretical investigation on the size effect of concrete compressive strength considering the maximum aggregate size, Int. J. Mech. Sci. 192 (2021) 106130, https://doi.org/10.1016/j.ijmecsci.2020.106130.
[53] Y. Wang, W. Zhang, G. Lou, T. Yao, Effect of limestone powder on mechanical properties of concrete based on Griffith's microcracking theory, Constr. Build. Mater. 449 (2024) 138413, https://doi.org/10.1016/j.conbuildmat.2024.138413.
[54] J. De Brito, R. Kurda, P.R. Da Silva, Can we truly predict the compressive strength of concrete without knowing the properties of aggregates? Appl. Sci. 8 (2018) 1095, https://doi.org/10.3390/app8071095.

[55] T. Özturan, C. Çeçen, Effect of coarse aggregate type on mechanical properties of concretes with different strengths, cem, Concr. Res. 27 (1997) 165–170, https://doi.org/10.1016/s0008-8846(97)00006-9.
[56] S. Kishore, L. Mounika, C. Maruti Prasad, B. Hari Krishna, Experimental study on the use of basalt aggregate in concrete mixes, ssrg Intern, J. Civ. Eng. 2 (2015) 37–40, https://doi.org/10.14445/23488352/ijce-v2i4p107.
[57] H.E. Yücel, M. Dutkiewicz, F. Yıldızhan, The effect of waste ballast aggregates on mechanical and durability properties of standard concrete, Mater 16 (2023) 2665, https://doi.org/10.3390/ma16072665.
[58] P.M. Shanmugavadivu, R. Malathy, D. Jegatheeswaran, Effect of gradation of manufactured sand in acid attack of concrete, Asian J. Chem. 26 (2014) S31–S35, https://doi.org/10.14233/ajchem.2014.19008.
[59] J. Huang, Z. Luo, M.B.E. Khan, Impact of aggregate type and size and mineral admixtures on the properties of pervious concrete: an experimental investigation, Constr. Build. Mater. 265 (2020) 120759, https://doi.org/10.1016/j.conbuildmat.2020.120759.
[60] C. Argiz, M.A. Sanjuán, R. Muñoz-Martialay, Effect of the aggregate grading on the concrete air permeability, Mater. Constr. 64 (2014) e026, https://doi.org/10.3989/mc.2014.07213.
[61] L. Basheer, P.A.M. Basheer, A.E. Long, Influence of coarse aggregate on the permeation, durability and the microstructure characteristics of ordinary Portland cement concrete, Constr. Build. Mater. 19 (2005) 682–690, https://doi.org/10.1016/j.conbuildmat.2005.02.022.
[62] R. Liu, H. Liu, F. Sha, H. Yang, Q. Zhang, S. Shi, Z. Zheng, Investigation of the porosity distribution, permeability, and mechanical performance of pervious concretes, Processes 6 (2018) 78, https://doi.org/10.3390/pr6070078.
[63] R. Yogesh, K. Santha, K. Ganesh, Synergistic effect of aggregate gradation band and cement to aggregate ratio on the performance of pervious concrete, J. Build. Eng. 73 (2023) 106718, https://doi.org/10.1016/j.jobe.2023.106718.
[64] H. Yang, R. Liu, Z. Zheng, H. Liu, Y. Gao, Y. Liu, Experimental study on permeability of concrete, IOP Conference Series. Earth Environ. Sci. 108 (2018) 022067, https://doi.org/10.1088/1755-1315/108/2/022067.
[65] G. Toplicic-Curcic, Z. Grdić, R. Ristic, I. Despotović, D. Dordevic, M. Dordevic, Aggregate type impact on water permeability of concrete, Romanian J. Mater. 42 (2012) 134–142.
[66] B.A. Warda, A.N. Munaz, Effects of aggregate gradation on water permeability of concrete, Adv. Mater. Res. 488–489 (2012) 248–252, https://doi.org/10.4028/www.scientific.net/amr.488-489.248.
[67] M. Naderi, A. Kaboudan, Experimental study of the effect of aggregate type on concrete strength and permeability, J. Build. Eng. 37 (2021) 101928, https://doi.org/10.1016/j.jobe.2020.101928.
[68] S.P. Yap, P.Z.C. Chen, Y. Goh, H.A. Ibrahim, K.H. Mo, C.W. Yuen, Characterization of pervious concrete with blended natural aggregate and recycled concrete aggregates, J. Cleaner Prod. 181 (2018) 155–165, https://doi.org/10.1016/j.jclepro.2018.01.205.
[69] S.I. Ahmad, M.A. Hossain, Water permeability characteristics of normal strength concrete made from crushed clay bricks as coarse aggregate, Adv. Mater. Sci. Eng. 2017 (2017) 1–9, https://doi.org/10.1155/2017/7279138.
[70] H.-B. Choi, J.-O. Park, Study on mechanical properties of concrete using basalt-based recycled aggregate and varying curing conditions, Mater 15 (2022) 4563, https://doi.org/10.3390/ma15134563.
[71] H.M. Al-Baijat, The use of basalt aggregates in concrete mixes in Jordan, Jordan, J. Civ. Eng. 2 (2008). https://elearning.just.edu.jo/jjce/issues/paper.php?p=40.pdf.
[72] N.N.M. Altwair, N.Y.O. Yacoub, N.A.M. Alsharif, N.L.S. Sryh, Influence of surface roughness on durability of new-old concrete interface, Adv. Technol. Innovation 9 (2024) 143–155, https://doi.org/10.46604/aiti.2024.13533.
[73] M. Jebli, F. Jamin, E. Malachanne, E. Garcia-Diaz, E. Youssoufi, Experimental characterization of mechanical properties of the cement paste aggregate interface in concrete, in: EPJ Web of Conferences, 140, 2017 12014, https://doi.org/10.1051/epjconf/201714012014.
[74] K. Newman, The effect of water absorption by aggregates on the water/cement ratio of concrete, Mag. Concr. Res. 11 (1959) 135–142, https://doi.org/10.1680/macr.1959.11.33.135.
[75] S. Al-Lami, Correlation between permeability and porosity with other properties of concrete, J. Appl. Eng. Sci. 19 (2021) 542–550, https://doi.org/10.5937/jaes0-27267.
[76] H. Kaur, N. Kulthaweepisit, T.N.H. Tran, C. Jaturapitakkul, W. Tangchirapat, Investigation of strength and water permeability of sustainable high-performance concrete containing high-volume ground bottom ash blended with fly ash and nano-silica, J. Build. Eng. 90 (2024) 109428, https://doi.org/10.1016/j.jobe.2024.109428.